

Preprint

Manuscript

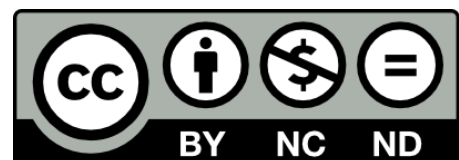
*Challenging the link between functional and
spectral diversity with radiative transfer
modeling and data*

Javier Pacheco-Labrador, Mirco Migliavacca, Xuanlong Ma,
Miguel D. Mahecha, Nuno Carvalhais, Ulrich Weber, Raquel
Benavides, Olivier Bouriaud, Ionut Barnoaiea, David A. Coomes,
Friedrich J. Bohn, Guido Kraemer, Uta Heiden, Andreas Huth,
Christian Wirth

2022

Published in Remote Sensing of Environment

<https://doi.org/10.1016/j.rse.2022.113170>



Challenging the link between functional and spectral diversity with radiative transfer modeling and data

Javier Pacheco-Labrador¹, Mirco Migliavacca^{2,1}, Xuanlong Ma^{3,4,5}, Miguel Mahecha^{6,7}, Nuno Carvalhais^{1,8}, Ulrich Weber¹, Raquel Benavides⁹, Olivier Bouriaud^{10,11}, Ionut Barnoaiea^{10,12}, David A. Coomes¹³, Friedrich J. Bohn^{14,15}, Guido Kraemer⁶, Uta Heiden¹⁶, Andreas Huth^{15,7,17}, Christian Wirth^{18,7,1}

¹ Max Planck Institute for Biogeochemistry, Hans Knöll Straße 10, Jena, D-07745, Germany

² current address: European Commission, Joint Research Centre (JRC), Ispra, Italy

³ College of Earth and Environmental Science, Lanzhou University, Lanzhou, Gansu, China 730000

⁴ International Research Center of Big Data for Sustainable Development Goals, Beijing, China, 100094

⁵ State Key Laboratory of Remote Sensing Science, Beijing Normal University, Beijing, China, 100875

⁶ Remote Sensing Center for Earth System Research, Leipzig University, Leipzig, Germany

⁷ German Centre for Integrative Biodiversity Research (iDiv), Halle-Jena-Leipzig, Germany

⁸ Departamento de Ciências e Engenharia do Ambiente, DCEA, Faculdade de Ciências e Tecnologia, FCT, Universidade Nova de Lisboa, 2829-516 Caparica, Portugal

⁹ Departamento de Sistemas y Recursos Naturales. E.T.S. Ingeniería de Montes, Forestales y del Medio Natural, Universidad Politécnica de Madrid, C/ José Antonio Novais 10, 28040, Madrid, Spain

¹⁰ University ‘Ștefan cel Mare’ of Suceava, Universităţii 13, Suceava 720229, Romania

¹¹ Laboratoire d’Inventaire Forestier, IGN, Nancy, France

¹² Geomatics Laboratory, Faculty of Forestry, University ‘Ștefan cel Mare’ Suceava, Romania

¹³ Department of Plant Sciences and the Conservation Research Institute, Downing Street, Cambridge, CB2 3EA, United Kingdom.

¹⁴ Department of Computational Hydrosystems, Helmholtz Centre for Environmental Research – UFZ, Leipzig, Germany

¹⁵ Department of Ecological Modelling, Helmholtz Centre for Environmental Research – UFZ, Leipzig, Germany

¹⁶ German Aerospace Center (DLR), Remote Sensing Technology Institute (IMF), Oberpfaffenhofen, 82234 Wessling, Germany

¹⁷ Institute of Environmental Systems Research, University of Osnabrück, Osnabrück, Lower Saxony, Germany

¹⁸ Systematic Botany and Functional Biodiversity, Leipzig University, Leipzig, Germany.

34 **Keywords:** Spectral diversity, functional diversity, radiative transfer model, biodiversity, Sentinel-2,
35 DESIS

36

37 **ABSTRACT**

38 In a context of accelerated human-induced biodiversity loss, remote sensing (RS) is emerging as a
39 promising tool to map plant biodiversity from space. Proposed approaches often rely on the Spectral
40 Variation Hypothesis (SVH), linking the heterogeneity of terrestrial vegetation to the variability of the
41 spectroradiometric signals. Yet, due to observational limitations, the SVH has been insufficiently tested,
42 remaining unclear which metrics, methods, and sensors could provide the most reliable estimates of plant
43 biodiversity. Here we assessed the potential of RS to infer plant biodiversity using radiative transfer
44 simulations and inversion. We focused specifically on “functional diversity,” which represents the spatial
45 variability in plant functional traits. First, we simulated vegetation communities and evaluated the
46 information content of different functional diversity metrics (FDMs) derived from their optical reflectance
47 factors (R) or the corresponding vegetation “optical traits,” estimated via radiative transfer model inversion.
48 Second, we assessed the effect of the spatial resolution, the spectral characteristics of the sensor, and signal
49 noise on the relationships between FDMs derived from field and remote sensing datasets. Finally, we
50 evaluated the plausibility of the simulations using Sentinel-2 (multispectral, 10 m pixel) and DESIS
51 (hyperspectral, 30 m pixel) imagery acquired over sites of the Functional Significance of Forest
52 Biodiversity in Europe (FunDivEUROPE) network. We demonstrate that functional diversity can be
53 inferred both by reflectance and optical traits. However, not all the FDMs tested were suited for assessing
54 plant functional diversity from RS. Rao’s Q index, functional dispersion, and functional richness were the
55 best-performing metrics. Furthermore, we demonstrated that spatial resolution is the most limiting RS
56 feature. In agreement with simulations, Sentinel-2 imagery provided better estimates of plant diversity than
57 DESIS, despite the coarser spectral resolution. However, Sentinel-2 offered inaccurate results at DESIS

58 spatial resolution. Overall, our results identify the strengths and weaknesses of optical RS to monitor plant
59 functional diversity. Future missions and biodiversity products should consider and benefit from the
60 identified potentials and limitations of the SVH.

61 **1. INTRODUCTION**

62 Human activities are leading to a massive and accelerated loss of Earth's life forms (Barnosky et
63 al. 2011; Ceballos et al. 2015); at the same time, the efforts to understand and prevent this loss still lack
64 global, continuous, and systematic information connecting biodiversity and its decline drivers (Hardisty et
65 al. 2019; Pereira et al. 2012). While remote sensing (RS) provides operational monitoring of some of the
66 major drivers of biodiversity variation at a global scale (e.g., land cover, land use, and climatic variables)
67 (Small and Sousa 2016; Sohl and Sleeter 2012; Yang et al. 2013), there are no comparable capabilities for
68 mapping plant biodiversity and its changes. A first step towards developing such a capability was the
69 definition of the Essential Biodiversity Variables, a set of "measurements required to study, report, and
70 manage biodiversity change" (c.f., (Pereira et al. 2013)). The Essential Biodiversity Variables are analogous
71 to the Essential Climate Variables (GCOS 2003), designed to understand and monitor climate change
72 (Scholes et al. 2012). The majority of Essential Climate Variables rely on RS to provide continuous and
73 systematic information over the whole Earth's surface (Yang et al. 2013). Similarly, RS is expected to
74 provide a significant fraction of the Essential Biodiversity Variables (Hardisty et al. 2019; Jetz et al. 2019).

75 The interest of the RS community in biodiversity has grown over the last decade in parallel with
76 advances in computer science and RS technology (Rocchini et al. 2010; Turner et al. 2003; Wang and
77 Gamon 2019). Biodiversity is a complex concept involving multiple facets: taxonomic as the diversity of
78 taxonomic groups (often species), phylogenetic as the branch length of the evolutionary tree of a
79 community, and functional as the diversity of functional traits; consequently, many RS-based Essential
80 Biodiversity Variables have been proposed (Skidmore et al. 2021). However, there is no clear community
81 consensus, as is the case for the meteorological and biophysical variables considered Essential Climate

82 Variables, about which EBVs should be taken forward. One of the most promising methods to assess
83 biodiversity from optical RS relies on the Spectral Variation Hypothesis (SVH), which states that the
84 variability of the spectral signals of a remote sensing image, termed “spectral diversity.”, should reflect the
85 spatial variation of the environment. The environmental heterogeneity would relate to the variability of
86 plant species, traits, and/or canopy structure (Palmer et al. 2002; Ustin and Gamon 2010), among other
87 factors (Rocchini et al. 2010; Wang and Gamon 2019). At the same time, plant diversity could relate to the
88 diversity of species of other *taxa* dependent on particular plant species (Jetz et al. 2019). According to Wang
89 and Gamon (2019), the main approaches proposed to quantify plant diversity from RS rely on a)
90 classification and mapping of individual species or broad functional types (Ibarrola-Ulzurrun et al. 2019;
91 Stagakis et al. 2016; Sun et al. 2019), b) classification and mapping of habitats (Kerr and Ostrovsky 2003;
92 Stein et al. 2014), c) estimation of vegetation traits (optical traits) and the analysis of their variability,
93 mimicking trait sampling in field surveys (Hauser et al. 2021a; Schneider et al. 2017; Torresani et al. 2021),
94 and d) direct analysis of the spectral diversity (Hauser et al. 2021b; Rocchini et al. 2021; Wang et al. 2018a;
95 Warren et al. 2014). The first two approaches, while valuable, strongly depend on the spatial scale and the
96 classification method. Limitations for classifying individual species are sometimes overcome by targeting
97 instead functional types, which might be too rigid to describe the ecosystem’s functionality (Van Cleemput
98 et al. 2021; Wang and Gamon 2019). Alternatively, the characterization of functional diversity might
99 provide a deeper insight into the biodiversity-ecosystem function relationships than taxonomic estimates
100 (Jetz et al. 2016). The last two approaches seek to characterize vegetation’s taxonomical, functional, and
101 even phylogenetic diversity through its spectral diversity or the diversity of optical traits derived from
102 spectral information (Cavender-Bares et al. 2020). Still, recent literature suggests that spectral and
103 taxonomic diversities might not be robustly correlated (Fassnacht et al. 2022). Nonetheless, most of these
104 methods have only been evaluated over relatively small extents (Féret and Asner 2014; Gholizadeh et al.
105 2018; Schneider et al. 2017; Schweiger et al. 2018; Torresani et al. 2019; Wang et al. 2018a), and as of now,
106 there are no comprehensive databases to assess their robustness and applicability in a global context.

107 RS missions must consider the trade-offs between spatial, spectral, and temporal resolutions
108 (Gamon et al. 2020). For biodiversity studies, pixel size should ideally allow the identification of individual
109 plants without being confounded by variability within the plant signal (e.g., shading and the presence of
110 different plant elements such as branches, soil, or understory vegetation) (Nagendra 2001; Nagendra and
111 Rocchini 2008). However, individual plants are typically smaller than pixels, which hampers the
112 characterization of biodiversity. For example, Wang et al. (2018a) explored how increasing pixel size
113 reduced spectral sensitivity to taxonomic diversity in a grassland. Alternatives to reduce the need for
114 accurate plant discrimination include fuzzy classification (Feilhauer et al. 2021), estimation of optical traits
115 at the resolution of the RS sensor (Torresani et al. 2021), or direct estimation of plant functional diversity
116 from spectral diversity (Ma et al. 2019). However, these approaches are still sensitive to sensor spatial
117 resolution since larger pixels integrate more species and traits and, therefore, more and more variability. At
118 the same time, mixing species can reduce the capability of retrieving vegetation optical traits (Darvishzadeh
119 et al. 2008). In addition, the sensor spectral configuration (resolution, sampling, and range) must provide
120 sufficient information to discriminate between different species or quantify optical traits. Hyperspectral
121 data continuously and finely resolve the spectral properties of Earth surfaces (Goetz 2009) and therefore
122 offer the best chances for successful classification (Dalponte et al. 2009; Sluiter and Pebesma 2010) or trait
123 retrieval (Lee et al. 2004; Lu et al. 2019). Nonetheless, spaceborne sensors must sacrifice either the spectral
124 or the spatial resolution, and it remains unresolved whether high-resolution multispectral or mid-resolution
125 hyperspectral missions are more useful for biodiversity assessment.

126 Spectral and functional diversities can involve multiple variables (i.e., plant traits or spectral bands).
127 Different authors have compared the variability of spectral signals in individual wavebands, combinations
128 of these, or averaged statistics in certain spectral regions (Féret and Asner 2014; Ma et al. 2019; Wang et
129 al. 2018a), as well as the variability of individual optical traits estimated from RS (Rossi et al. 2020;
130 Torresani et al. 2021) with field biodiversity data. Alternatively, ecologists have proposed several functional
131 diversity metrics (FDMs) to summarize the information in multidimensional datasets of species traits. These

132 metrics quantify different aspects of functional diversity (i.e., richness, evenness, and divergence) with
133 single scalars (Laliberté and Legendre 2010; Mason et al. 2005; Villéger et al. 2008). The computation of
134 FDMs often requires removing the covariance between variables (Anderson 2006); however, despite the
135 abstraction, FDMs are informative and sensitive to underlying assembly processes (Mouchet et al. 2010).
136 Typically, FDMs are constructed from plant functional trait data collected in the field (e.g., measurements
137 of pigment and mineral nutrient concentrations taken on leaf samples). These metrics can also be computed
138 from RS variables such as spectral reflectance factors and optical traits (Schneider et al. 2017; Torresani et
139 al. 2019), being possible to replace taxonomic species with the “spectral species” concept (Féret and Asner
140 2014). What remains unclear is to what extent FDMs computed from spectral data or optical traits can be
141 translated to FDMs computed from vegetation functional traits collected in the field, and the role of the
142 spectral configuration (resolution, sampling, and range), spatial resolution, and signal noise.

143 So far, the SVH has been inconsistently tested. The works mentioned above evaluated the potential
144 of different metrics, methods, and sensors with little overlap, preventing a solid comparison of their
145 performance. Moreover, the lack of accurate validation data covering broad ranges of traits and
146 communities consistently imaged by multiple sensors of well-known uncertainties has limited the
147 generalization of the results. To overcome these issues, we evaluate the potential of different FDMs to relate
148 spectral and functional diversity using both synthetic and observational datasets. Our study aims to answer
149 the following questions: a) Which remote sensing-based FDMs are able to capture functional diversity from
150 field plant traits? b) What are the advantages and disadvantages of computing FDMs directly on the spectral
151 reflectance factors (R) or optical traits (T_{optical}) estimated via radiative transfer model (RTM) inversion? c)
152 Are the relationships between field and remote sensing-based FDMs consistent when compared at local and
153 global scales? d) How do RS features such as spectral configuration, spatial resolution, and signal noise
154 affect the relationships between vegetation and remote sensing-based FDMs? To answer these questions,
155 we first developed an RTM simulation framework that allowed us to produce synthetic vegetation
156 communities and the related spectral signals featuring different spectral and spatial configurations and

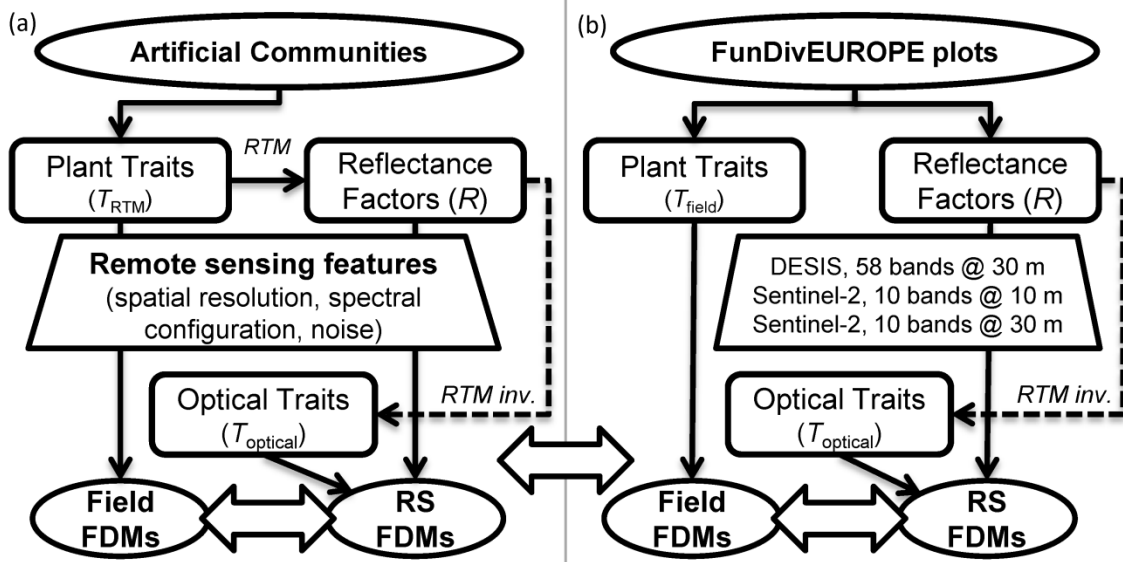
157 noise. Then, using these simulations, we evaluated and compared two common RS methods to map
158 functional diversity: spectral signals (i.e., reflectance factors) or optical traits estimated from inverse
159 modeling. Finally, we evaluated the coherence of the simulation results using DLR Earth Sensing Imaging
160 Spectrometer (DEGIS) and Sentinel-2 imagery and field taxonomic and functional diversity estimates from
161 forest plots of the Functional Significance of Forest Biodiversity in Europe (FunDivEUROPE) network
162 (Baeten et al. 2013).

163

164 **2. METHODS**

165 Fig. 1 summarizes the simulation and data analysis workflows. First, we simulated artificial
166 communities of plant species, each defined by a unique set of traits (i.e., RTM parameters) and the
167 individual species' reflectance factors using an RTM. Then, we applied different RS features (spatial
168 resolution, spectral configuration, and noise) to the reflectance factors to represent how different remote
169 sensors perceived the plant communities. Using this simulation framework, we evaluated the relationships
170 between quantitative FDMs computed from the plant traits (as could be measured in the field) and RS
171 variables (either reflectance factors or optical traits estimates) and how these were affected by the RS
172 features (Fig. 1a, section 2.3). Finally, we analyzed different sets of satellite imagery acquired over
173 FunDivEUROPE biodiversity monitoring plots and assessed if the relationships between field and remote
174 sensing FDMs were coherent with the former simulations (Fig. 1b, section 2.4).

175



176

177 Figure 1. Flowchart outlining analyses of simulated (a) and observational data (b) to assess the capability of
 178 different functional diversity metrics (FDMs) to link spectral and vegetation functional diversity and the effect of
 179 different remote sensing features. Solid lines indicate the direct use of the data or models; dashed lines indicate the
 180 inverse use of a radiative transfer model (RTM). In the simulations (a), some analyses include the effects on plant
 181 traits of added noise and different spatial resolutions.

182

183 2.1 Functional diversity metrics

184 We evaluated the capability of Functional richness (*FRic*), evenness (*FEve*), diversity (*FDiv*),
 185 dispersion (*FDis*), and Rao's quadratic entropy Q (*RaoQ*) metrics (Botta-Dukát 2005; Laliberté and
 186 Legendre 2010; Villéger et al. 2008) to connect field and RS-based functional diversity. These metrics were
 187 computed with the *dbFD* R-package (Laliberté and Legendre 2010) using traits Euclidean distance as the
 188 dissimilarity measure. The package applies standardization of the variables and Principal Coordinates
 189 Analysis (Anderson 2006) on the distance matrix to remove the influence of variables' magnitude and
 190 redundant information, respectively. Moreover, we used a parametric formulation of Rao's Q (Eq. 1) as
 191 proposed by Rocchini et al. (2021) with values of the parameter α , ranging from 0 to infinity. In this case,
 192 we first applied standardization and principal component analysis (PCA) (Pearson 1901) to the traits before

193 computing the Euclidean distance, keeping only the components that explained 98 % of the variance in
194 total. This approach allowed us to reduce the number of variables and evaluate the effect of noise (section
195 2.3.4).

196

$$\text{Rao}Q_\alpha = \left(\sum_{i,j}^N p_i p_j d_{ji}^\alpha \right)^{\frac{1}{\alpha}} \quad (1)$$

197

198 where i and j are indices for each species in the community, p their respective probabilities, and d is a
199 symmetric measure of multidimensional distance between the species traits or, in this case, a set of their
200 principal components.

201 We computed these FDMs from remote sensing variables that were either reflectance factors or
202 optical traits estimated by inverting an RTM against the reflectance factors (T_{optical} , section 2.3.4 and 2.4.3).
203 We also used plant traits at the field level (“field plant traits”), either inputs of the RTM used to simulate
204 reflectance factors (T_{RTM} , section 2.2) or sampled in the FunDivEUROPE plots (T_{field} , section 2.4.1). Notice
205 that not all of these traits are “functional traits” *sensu* Díaz and Cabido (2001), but vegetation characteristics
206 or structural state variables as they are not species-specific and change with ontogeny, environment, and
207 forest management (e.g., canopy height or leaf area index). Still, we used these traits since ecologists have
208 selected them to characterize functional diversity in mature forests (i.e., T_{field}) (Baeten et al. 2013; Benavides
209 et al. 2019a; Benavides et al. 2019b), or since modelers use them to describe light-vegetation interaction
210 (i.e., T_{RTM}) (North 1996; Verhoef 1985). The implications of this choice are discussed in section 4.4.

211

212 **2.2 Radiative transfer model and emulation**

213 RTMs describe light-matter interaction. They mechanistically link vegetation parameters (here
214 referred to as traits), describing plant structure and biochemistry with the spectral signals perceived by
215 remote sensors. Therefore, RTMs allow simulating canopy reflectance factors from a set of model
216 parameters and retrieving plant traits from spectral observations through inverse modeling (Jacquemoud et
217 al. 2009). In this work, we used the Soil Canopy Observation, Photochemistry and Energy fluxes (SCOPE)
218 model (van der Tol et al. 2009) to simulate vegetation's optical properties as a function of plant traits (i.e.,
219 T_{RTM}). SCOPE includes the leaf RTM Fluspect-CX (Vilfan et al. 2018), which incorporates anthocyanins
220 specific absorption coefficients from PROSPECT-D (Féret et al. 2017). SCOPE T_{RTM} includes 1) leaf traits
221 such as the number of internal leaf layers (N , layers), and chlorophyll a and b (C_{ab} , $\mu\text{g cm}^{-2}$), carotenoids
222 (C_{ca} , $\mu\text{g cm}^{-2}$), anthocyanins (C_{ant} , $\mu\text{g cm}^{-2}$), senescent pigments (C_{s} , a.u.), dry matter (C_{dm} , g cm^{-2}) and water
223 (C_{w} , g cm^{-2}) contents; and 2) traits describing vegetation structure as the mean and bimodality of the leaf
224 inclination distribution function ($LIDF_a$ and $LIDF_b$, respectively), leaf area index (LAI , $\text{m}^2 \text{m}^{-2}$), canopy
225 height (h_c , m), and the leaf width (l_w , m). Additional model parameters describing soil optical properties
226 and illumination-observation conditions are described in Table S1.

227 In addition, we used statistical models or emulators (Gómez-Dans et al. 2016) to enable fast
228 computation of large datasets of reflectance factors with SCOPE. We trained and validated two shallow
229 neural networks predicting specie's reflectance factors from their traits, each with a different set of look-up
230 tables. We used the first for simulation (section 2.3.3) and the second to retrieve optical traits via RTM
231 inversion (section 2.3.4). Using two different emulators allowed us to force a model error in the retrieval,
232 making it more realistic (Supplementary SM1 and Table S2 describe the emulators' training and comparison
233 and present their statistics, respectively).

234

235 **2.3 Simulation of traits and spectral diversity**

236 Fig. 2 represents a schematic with the details of the simulation of synthetic vegetation communities
 237 and their spectral signals, the simulation of different remote sensing features on these signals, and the
 238 various comparisons of the FDMs computed from field plant or remote sensing data.
 239

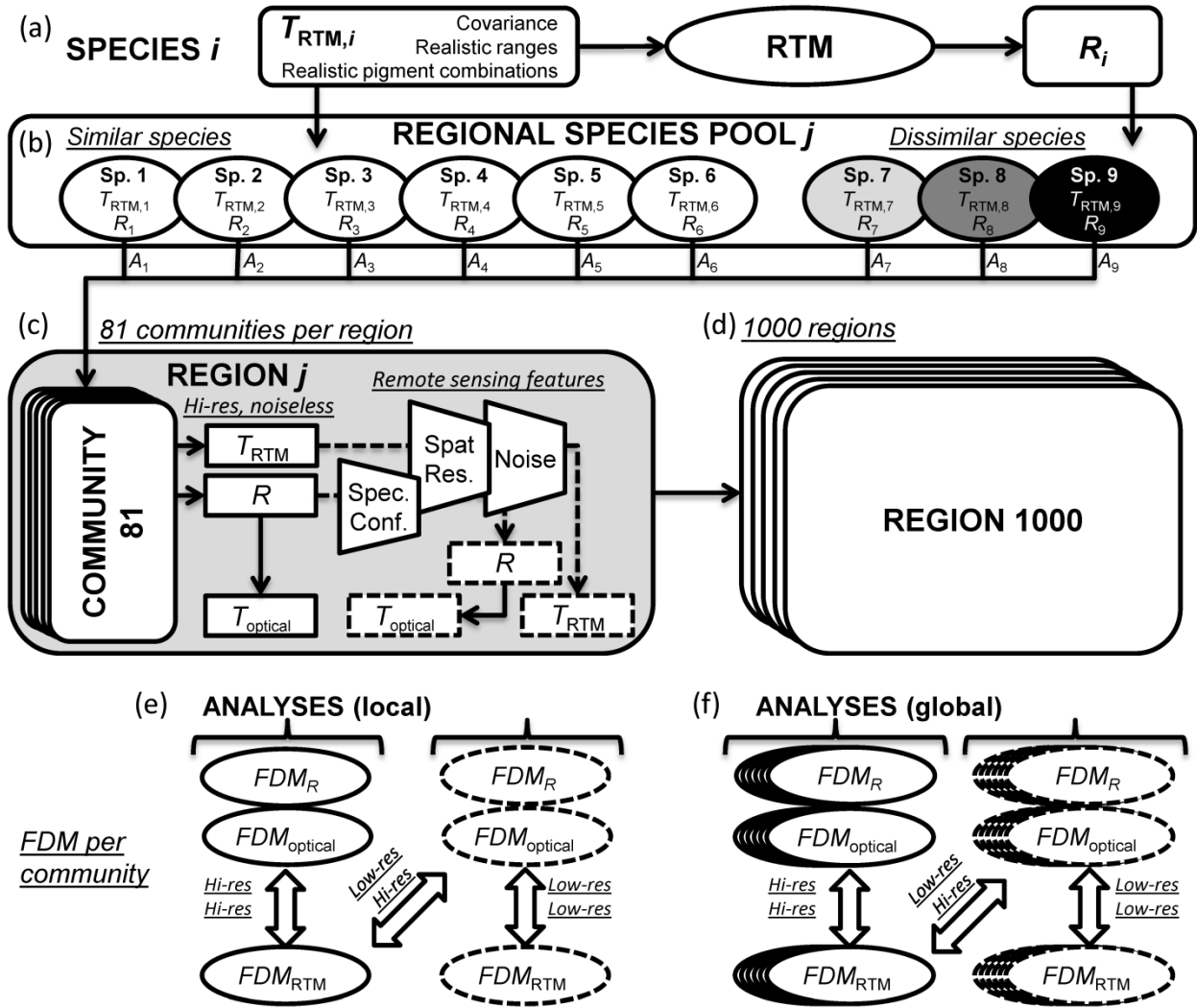


Figure 2. Detailed simulation and analysis workflow. Each species (i) is defined by a plausible set of field plant traits (T_{RTM}), the input of a radiative transfer model (RTM) that predicts the associated reflectance factor (R) (a). Several species (9 in this example) are gathered within a regional species pool (b). Some species feature traits with close or similar values (similar species), whereas others feature dissimilar trait values (dissimilar species). Then, the species from the pool are sampled with different abundances (A) to produce 81 communities per region (c); the original

traits and reflectance factors (solid lines) are transformed by different remote sensing features (dashed lines). In both cases, the plant traits are also estimated from the optical signals via radiative transfer model inversion (optical traits, T_{optical}). In total, 1000 regions are produced from a corresponding number of species pools (d). Functional diversity metrics (FDM) are computed from the abundances and either the field vegetation traits (FDM_{RTM}), the optical traits (FDM_{optical}), or the spectral reflectance factors (FDM_R) of each community. The relationships between the FDMs at different spatial resolutions are compared for each region (e) and all the regions at the same time (f)

240

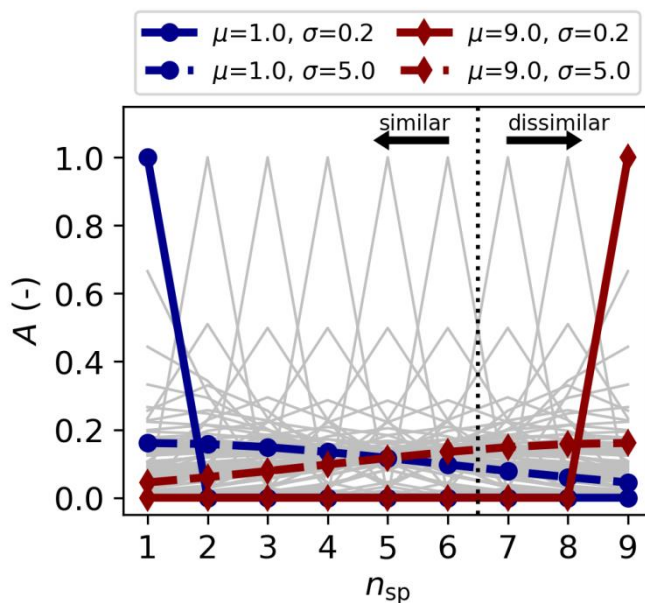
241 2.3.1 Species, communities, and regions

242 We defined each synthetic plant species with 1) a unique set of plausible biochemical and structural
243 traits (i.e., T_{RTM}) and 2) the corresponding reflectance factors predicted by the emulator (Fig. 2a). Field
244 plant traits were randomly sampled; however, we ensured plausible combinations of traits by accounting
245 for known ranges in different types of vegetation (e.g., forests, crops, grasslands, etc., reported in Table S1)
246 and traits covariance identified in spectral libraries (Appendix A). Since we emulated a unidimensional
247 RTM, we did not further describe these species (e.g., stem type or crown shape) nor attempted to focus on
248 any specific vegetation type or ecosystem. The limitations of the modeling framework are discussed in
249 section 4.3.

250 Between 5 and 30 synthetic species were gathered to produce regional species pools (Fig. 2b). The
251 pools contain all the species present in a region (or remote sensing image) that mix later in different
252 communities (or moving windows used for image analysis). In practice, the pools are a species-by-traits
253 matrix containing the traits (i.e., T_{RTM}) of the species present in a region. In nature, biotic and abiotic
254 filtering and interactions determine species assemblages according to their traits (Jucker et al. 2018). These
255 processes can prevent or enable the combination of traits with very similar or very different values in the
256 same community. Therefore, we ensured assemblage variability by different fractions of similar and
257 dissimilar species in the pools. We forced part of the pool species to be similar by sampling their traits
258 within narrow ranges. For example, chlorophyll content (C_{ab}) could be limited between 20 and 30 $\mu\text{g cm}^{-2}$.

259 In contrast, we also produced dissimilar species by sampling their traits within wide plausible bounds (0-
 260 $100 \mu\text{g cm}^{-2}$ for C_{ab} in Table S1). The fraction of similar and dissimilar species and the width of the sampling
 261 range for the similar species were randomly set. We set the same soil properties for all the species for each
 262 pool, but these varied between pools. Contrarily, we fixed a constant diffuse-to-global radiation ratio (δ_{DG}
 263 $= 0.20$) and sun zenith angle ($\theta_{\text{sun}} = 30^\circ$) for all the simulations.

264 Finally, we simulated 81 communities per region by combining the regional pool species with
 265 different relative abundances (A) (Fig. 2c). First, we numbered the species, clustering similar and dissimilar
 266 species separately (e.g., in Fig. 2b, similar species range from 1 to 6, and dissimilar species from 7 to 9).
 267 Then we assigned the abundances using the probability predicted by a Gaussian distribution for these
 268 numbers maximizing the range of possible combinations of the species pool (Appendix B). To do so, we
 269 gradually modified the dominant species (the mean) and the degree of dominance (the standard deviation)
 270 of each community. Fig. 3 exemplifies the relative abundances of the 81 communities produced for the
 271 species pool in Fig. 2b and highlights the most extreme cases.



272

Figure 3. Example of the relative abundances (A) simulated for the regional species pool in Fig. 2b (9 species). The species are indexed with integer values (n_{sp}), separating similar from dissimilar species. The relative abundances are

generated by gridding the mean (μ) and standard deviation (σ) of the Gaussian distribution assigning species abundances. The figure highlights the most extreme cases where species 1 (similar) or 9 (dissimilar) are dominant (determined by μ), with maximum and minimum degrees of dominance (with $\sigma = 0.2$ and $\sigma = 5.0$, respectively).

273 2.3.2 Remote sensing features

274 We evaluated the effects of three features of the RS data on the relationships between FDMs (Fig.
 275 2c): 1) spectral resolution and configuration (i.e., bands width, range, location), 2) spatial resolution, and
 276 3) signal noise. Since field data are also uncertain, we applied the same noise level to reflectance factors
 277 and field plant traits (Fig. 2c). We simulated three levels for each RS feature and tested all the possible (27)
 278 combinations (Table 1). This analysis envisaged evaluating the trade-offs between different mission
 279 concepts to study functional diversity from space.

280

Table 1. Remote sensing features tested in the simulation analysis. The noise level reported was applied to the simulated reflectance factors and the field plant traits. Regarding the spectral configuration, DESIS and Sentinel-2 Multi-Spectral Instrument (MSI) spectral response functions were obtained from imagery metadata (section 2.4.1) and the European Space Agency (ESA 2017), respectively. The first row presents the ideal combination of features (maximum resolution, noiseless) on which the rest of the simulations are based.

Spectral configuration	Spatial Resolution	Noise
<u>Full-hyperspectral</u> 2001 bands between 400-2400 nm, 1 nm step	<u>High: S_{res,100}</u> All the species of the community are individually discriminated	<u>Low: $\sigma_{\text{noise}} = 0 \%$</u> Noiseless signal
<u>DESI</u> 58 bands (4x binned) between 410-986 nm	<u>Medium: S_{res,50}</u>	<u>Medium: $\sigma_{\text{noise}} = 5 \%$</u> 5 % of Gaussian noise

	Half of the species of the community are observed as a mixture	
<u>Sentinel-2</u> 10 bands between 490-2190 nm	<u>Low: $S_{res,0}$</u> None of the species of the community can be individually identified; they are all mixed by the sensor	<u>High: $\sigma_{noise} = 10 \%$</u> 10 % of Gaussian noise

281

282 Species' reflectance factors were initially simulated at 1 nm step between 400 and 2400 nm ("full-
 283 hyperspectral") and then convolved to the spectral bands of two different sensors: DESIS and Sentinel-2.
 284 DESIS is a visible and near-infrared hyperspectral imager onboard the International Space Station (Kerr et
 285 al. 2016). Sentinel-2 is one of the Copernicus missions managed by the European Space Agency (ESA). It
 286 carries the Multi-Spectral Instrument (MSI), a visible, near, and short-wave infrared multispectral imager
 287 that maps Earth's surface properties with ten wavebands (Drusch et al. 2012).

288 Since our simulation did not describe the spatial distribution of the species within each community,
 289 we defined the spatial resolution as the sensor's capability to discriminate between individual species and
 290 their spectral signatures. Initially, the simulations represented highly resolved imagery, providing an
 291 accurate characterization of each species and their abundances in the community ($S_{res,100}$). Then we ran two
 292 additional simulations where the sensor could only discriminate half ($S_{res,50}$) or none of the community
 293 species ($S_{res,0}$). In these cases, new species were perceived as a linear combination of the reflectance factors
 294 and the abundances of the species that could not be distinguished (Appendix C). In addition, we applied the
 295 same transformation to the field plant traits (T_{RTM}) to compare field and RS data at the same spatial
 296 resolution (section 2.3.5).

297

298 2.3.3 Simulations

299 In total, we produced 27 simulations (all the column combinations in Table 1), each consisting of
300 1,000 species pools and 81 communities (thus 81,000 communities), integrating a total of 16,153 species
301 (Fig. 2d). For comparison, we initialized all the simulations with the same noiseless and full spectral and
302 spatial resolution abundances, reflectance factors, and field plant traits (Table 1, first row). Then, these were
303 modified by combinations of the different levels of the RS features to assess their effect on the relationships
304 between field and remote sensing FDMs. Fig. 4a-c exemplifies the simulation of a synthetic community
305 (similar and dissimilar specie's abundances, spectra, and traits, respectively) and the role of the RS features
306 (Fig. d-i). The degradation of the spatial resolution modifies the sensor's perception of the abundances (Fig.
307 4a,d,g) and spectral properties (Fig. 4b,e,h). When pixels become larger, they can include new species from
308 outside the area occupied by the community (or a reference field plot (Gholizadeh et al. 2018)). From a
309 remote sensing perspective, these communities could just be moving windows where pixels are selected to
310 compute FDMs (e.g., Rocchini et al. (2021)). Moreover, the mixture of spectral signals can hide the
311 signature of the rarest species, reduce the representativeness of locally dominant species, and, overall,
312 reduce spectral diversity in the region. At the same time, the convolution to spectral bands of different
313 sensors reduces the detail and extent of the spectral data. In contrast, noise increases variability (Fig. 4e,h
314 vs. Fig. 4f,i).

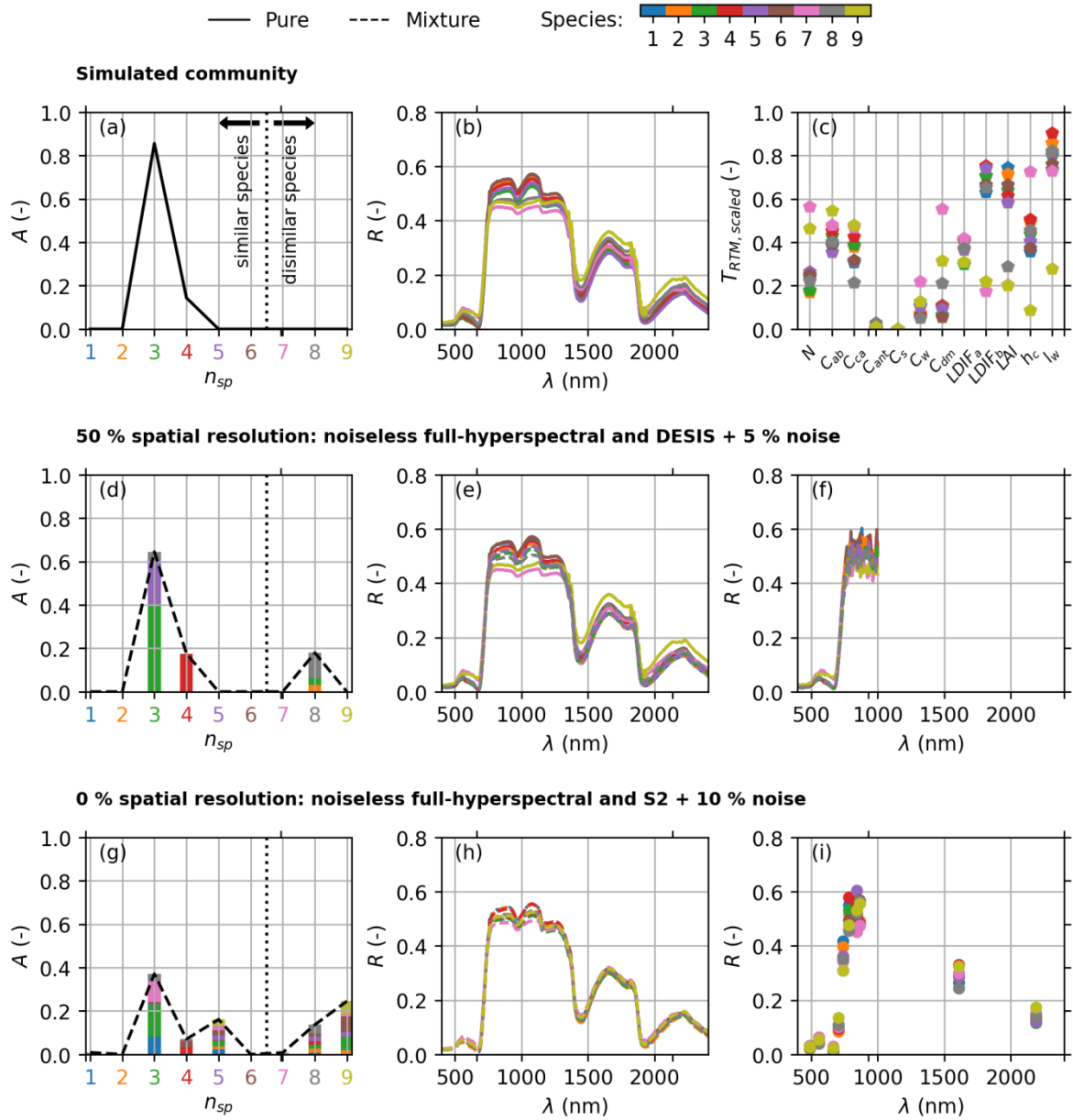


Figure 4. Example of the simulation of a synthetic community and effect of different remote sensing features on the perception of specie's reflectance factors and abundances. The first row presents the original abundances (A) (a), species reflectance factors (R) (b), and field plant traits (T_{RTM}) scaled within the bounds set for the simulation (c). In the abundance subplots (first column), the black-pointed line separates similar (on the left) from dissimilar species (on the right). The color assigned to each species' number (n_{sp}) identifies the corresponding reflectance factors and traits in the remaining subplots. Solid lines represent pure species, whereas dashed lines represent spectral mixtures

due to spatial resolution degradation. The second row degrades spatial resolution so that only 50 % of the species in the pool can be discriminated, leading to new estimates of species abundances (d); the color bars represent the contribution of each species to the new species abundance, as observed by the remote sensor. Sensed reflectance factors, full-hyperspectral and noiseless (e), or convolved to DESIS spectral bands with a 5% random noise (f). The third row degrades spatial resolution so that none of the species can be identified, leading to new estimates of species abundances (g); the color bars represent the contribution of each species to the new species abundance, as observed by the remote sensor. Sensed reflectance factors, full-hyperspectral and noiseless (e), or convolved to Sentinel-2 MSI spectral bands with a 10% random noise (i).

315

316 2.3.4 Retrieval of optical traits

317 We estimated optical traits from the species' reflectance factors via inversion of the emulated RTM
318 (T_{optical}) for each of the 27 simulations (Fig. 2c). This way, we accounted for the effect of the different remote
319 sensing features on the retrieval. Additionally, using a second emulator for the inversion, we accounted for
320 model error (models' inaccuracy or limitation to represent the observation) since both emulators predict
321 slightly different reflectance factors for the same input. This approach does not aim to analyze or quantify
322 the effect of different model structures and vegetation features in the inversion of RTMs, but to include a
323 plausible source of uncertainty inherent to RTM inversion. We estimated the optical traits using a numerical
324 optimization approach (Jacquemoud et al. 2009) in two steps. First, we calculated an initial solution using
325 a look-up table approach. Then, the most relevant vegetation parameters were further optimized using the
326 L-BFGS-B algorithm (Zhu et al. 1997) (Supplementary SM2 provides a complete description).

327

328 2.3.5 Functional diversity metrics computation and comparison

329 For each simulation (27), we computed the FDMs from field plant traits (T_{RTM} , as if measured in
330 the field) and remote sensing data (reflectance factors or optical traits estimated via model inversion). FDMs
331 were independently computed for the 81 communities of each region as described in section 2.1 (Fig. 2e).

332 We analyzed the relationships between field-based (T_{RTM}) and RS-based (R or $T_{optical}$) metrics to understand
333 their ability to capture vegetation functional diversity from space. Linear models were evaluated using the
334 coefficient of determination (R^2) and the normalized root mean squared error ($NRMSE$, normalized by the
335 95 % confidence interval of the dependent variable to reduce the effect of outliers).

336 Also, we evaluated FDM relationships at global and local scales to understand their consistency
337 and applicability in both contexts. First, we compared at once all the species pools of each simulation
338 (global, 81 communities by 1,000 species pools) to assess their capability to provide information
339 comparable between different ecosystems, regions, or RS images (Fig. 2f). Then we compared the FDMs
340 of the communities of each species pool separately (local, 1,000 species pools) and extracted the median
341 and the 95 % confidence interval of the statistics (Fig. 2e). This second comparison studied the capability
342 of each FDM to infer functional diversity within a single ecosystem, region, or image.

343 In addition, we evaluated the effect of the resolution at which field traits are sampled and compared
344 with RS metrics (Fig. 2e,f). On the one hand, we compared field FDMs at maximum spatial resolution (hi-
345 res) to simulate the mismatch between imagery and field surveys characterizing individual species (this
346 means field $S_{res,100}$ vs. remote sensing $S_{res,50}$ or $S_{res,0}$). This analysis simulates the case where ecology studies
347 characterizing individual species are combined with remote sensing data, as in section 2.4. On the other
348 hand, we compared vegetation FDMs at the spatial resolution of the sensor (RS-res, comparing $S_{res,50}$ vs.
349 $S_{res,50}$ or $S_{res,0}$ vs. $S_{res,0}$, respectively). Here, we simulated field surveys characterizing vegetation within plots
350 specifically designed to match satellite pixels (e.g., Hauser et al. (2021a; 2021b)) but not identifying
351 individual species. This second analysis represents the case of typical remote-sensing oriented surveys
352 where field datasets are integrated, mimicking the remote sensor's spatial resolution.

353 For all these cases, we compared the FDMs' performance of the 27 simulations to understand the
354 effect of the remote sensing features and signal noises under evaluation.

355

356 2.4 Estimation of functional diversity with DESIS and Sentinel-2 at FunDivEUROPE sites

357 2.4.1 Study sites and field-based biodiversity metrics

358 We combined field and RS data collected in plots of the FunDivEUROPE network
359 (<http://www.fundiveurope.eu>) (Baeten et al. 2013; Benavides et al. 2019a; Benavides et al. 2019b). The 30
360 x 30 m plots covered matured forests in Spain (Mediterranean oak and pine woodland) and Romania
361 (mountainous mixed conifer and beech). The other network regions were discarded from the analysis since
362 they were not covered by DESIS (i.e., Finland) or because foliar traits had not been measured (Ma et al.
363 2019). In each country, the plots were located to cover the local diversity gradients of the pool of (up to
364 four) dominant tree species, covering 5 x 5 km and 50 x 50 km regions in Romania and Spain, respectively.
365 FunDivEUROPE design ensured the inclusion of different levels of taxonomic richness, each
366 comprehending different mixtures of species and sufficient representativeness of each species featuring
367 similar frequencies (Baeten et al. 2013). Plant traits were measured in the dominant tree species, and field-
368 based FDMs were computed in plots where dominant species covered more than 95 % of the abundance
369 (Ma et al. 2019).

370 In each plot, ten trees per species with a diameter at breast height (DBH , m) larger than 7.5 cm were
371 selected to measure DBH , h_c (tree height), and crown cross-sectional area ($CCSA$, cm^2). LAI was determined
372 for the whole plot with an LAI-2000 Plant Canopy Analyzer (LI-COR, Lincoln, NE, USA), as described in
373 Grossiord et al. (2014), and therefore it was not used to compute field FDMs. Moreover, a top south-facing
374 branch was cut per tree, and around ten leaves per branch were sampled. Half of them were used to
375 determine leaf nitrogen concentration (N_{mass} , %) and leaf carbon concentration (C_{mass} , %). The other half
376 was used to determine leaf area (l_a , mm^2), specific leaf area (SLA , $mm^2\ mg^{-1}$), and leaf dry matter
377 concentration ($LDMC$, $mg\ g^{-1}$) (Benavides et al. 2019a; Benavides et al. 2019b). In total, 1763 trees were
378 sampled. The field campaigns took place in July in Romania 2013 and June 2013 in Spain.

379 We did not compute the FDMs in the *dbFD* package on these field-measured traits since *FRic* and
 380 *FDiv* require more species than traits, and the maximum plot richness is four. Instead, we applied
 381 standardization, PCA, and computed parametric Rao’s Q . As before, we kept the components explaining
 382 98 % of the variance. We also calculated two taxonomic diversity metrics: the Shannon index (H) and
 383 species richness (S). Where S equals the number of species in the plot (up to 4), and H predicts the
 384 uncertainty of guessing the species of individuals randomly sampled from the community (Shannon 1948).
 385 H (Eq. 2) increases as the community’s richness and evenness do.
 386

$$H = - \sum_{i=1}^S A_i \log(A_i) \quad (2)$$

387

388 2.4.2 Imagery and reflectance-based biodiversity metrics

389 We analyzed DESIS and Sentinel-2 imagery acquired over the FunDivEUROPE plots described in
 390 section 2.4.1. Following Ma et al. (2019), we used for all the analyses Sentinel-2 imagery acquired in the
 391 summer of 2015 since it was the closest to field sampling. However, DESIS imagery corresponds to the
 392 summer of 2020. Therefore, to improve DESIS and field data comparability, we also processed Sentinel-2
 393 imagery acquired in the summer of 2020 and used these images to discard field plots that substantially
 394 changed after 2015 (Supplementary SM3) and assess the effect of the temporal gap on the evaluation of
 395 DESIS in FunDivEUROPE. Table 2 summarizes the imagery used and the number of plots selected
 396 according to their temporal stability, absence of clouds, and field data availability.

397

398 Table 2. DESIS and Sentinel-2 imagery selected over FunDivEUROPE plots. Mean atmospheric optical thickness
 399 (AOT), sun zenith (θ_{sun}), view zenith (θ_{view}), and azimuth phase ($\Delta\phi$) angles of the plots selected are also presented.

Country	Date	Plots	Mean θ_{sun}	Mean θ_{view}	Mean $\Delta\phi$	Mean AOT
---------	------	-------	----------------------------	-----------------------------	-------------------	------------

		selected				
DEGIS						
Spain	2020-Jun-29 10:11	14	30.8	23.9	6.6	0.264
Romania	2020-Jun-29 07:02	8	45.9	2.1	3.7	0.283
Sentinel-2						
Spain	2015-Jul-29 11:00	25	2.6	26.1	121.0	0.015
Romania	2015-Jul-29 09:20	19	5.8	30.7	121.5	0.014
Spain	2020-Jun-22 10:56	23	2.7	21.5	127.5	0.082
Romania	2020-Jul-09 09:06	11	9.2	28.1	51.6	0.081

400

401 We downloaded DESIS L2A products from the EOWEB[®] GeoPortal (<https://eoweb.dlr.de/egp/>);

402 standard radiometric, atmospheric, and terrain corrections were automatically applied by DLR (Alonso et

403 al. 2019). During download, we applied nearest-neighbor resampling and a default ozone column value of

404 330 Dobson units. Metadata files provided the average atmospheric optical thickness (*AOT*) sensor height

405 and sun and view angles at the scene’s center, from which we calculated the corresponding angles on each

406 plot. Sentinel-2 images were processed using the ESA’s Sen2Cor processor (v2.2.0,

407 <https://step.esa.int/main/third-party-plugins-2/sen2cor/>) to produce L2A bottom of the atmosphere

408 reflectance factors. Then we pan-sharpened the 20-m bands (B05-B07, B8A, B11, and B12) to 10 m spatial

409 resolution using the unmixing method developed by Brodu (2017) and implemented in the ESA’s Sen2Res

410 toolbox (<http://step.esa.int/main/snap-supported-plugins/sen2res/>). Further details of Sentinel-2 imagery

411 processing can be found in Ma et al. (2019). Next, we obtained the corresponding *AOT* from the products

412 of the atmospheric correction and estimated all the sun and view angles using the python package

413 *sentinel2_angle_bands* (https://github.com/brazil-data-cube/sentinel2_angle_bands). Then, we resampled

414 Sentinel-2 to DESIS spatial resolution to understand to what extent the differences between the functional
415 diversity estimates of each mission could be related to their spatial or spectral features.

416 We extracted the 3 x 3 pixels windows centered on each FunDivEUROPE plot with spatial
417 resolutions of 10 (S2₁₀) and 30 m (S2₃₀ and DESIS). We gathered these data to get single standardization
418 and PCA models for each sensor, keeping the components that explained 98 % of the variance to reduce
419 signal noise. Then we computed the FDMs described in section 2.1; in this case, each pixel of the 3 x 3
420 window was considered a unique species whose abundance was the inverse of the number of pixels in the
421 window, as described in Rocchini et al. (2021). Fig. 5 shows an example of the spectral data available in
422 one of the FunDivEUROPE sites in Spain for S2₁₀ (Fig. 5a,d), S2₃₀ (Fig. 5b,e), and DESIS (Fig. 5c,f). S2₁₀'s
423 high spatial resolution allows sampling the internal variability of the field plot with a 3 x 3 window; DESIS
424 resolution equals the plot size (30 m) and instead samples the variability of the surroundings of the plot.
425 Also, DESIS more finely captures the visible and near-infrared region's variability, whereas Sentinel-2
426 captures a larger spectral diversity in the short-wave infrared. These differences can be observed both in
427 the imagery and the spectra.

428

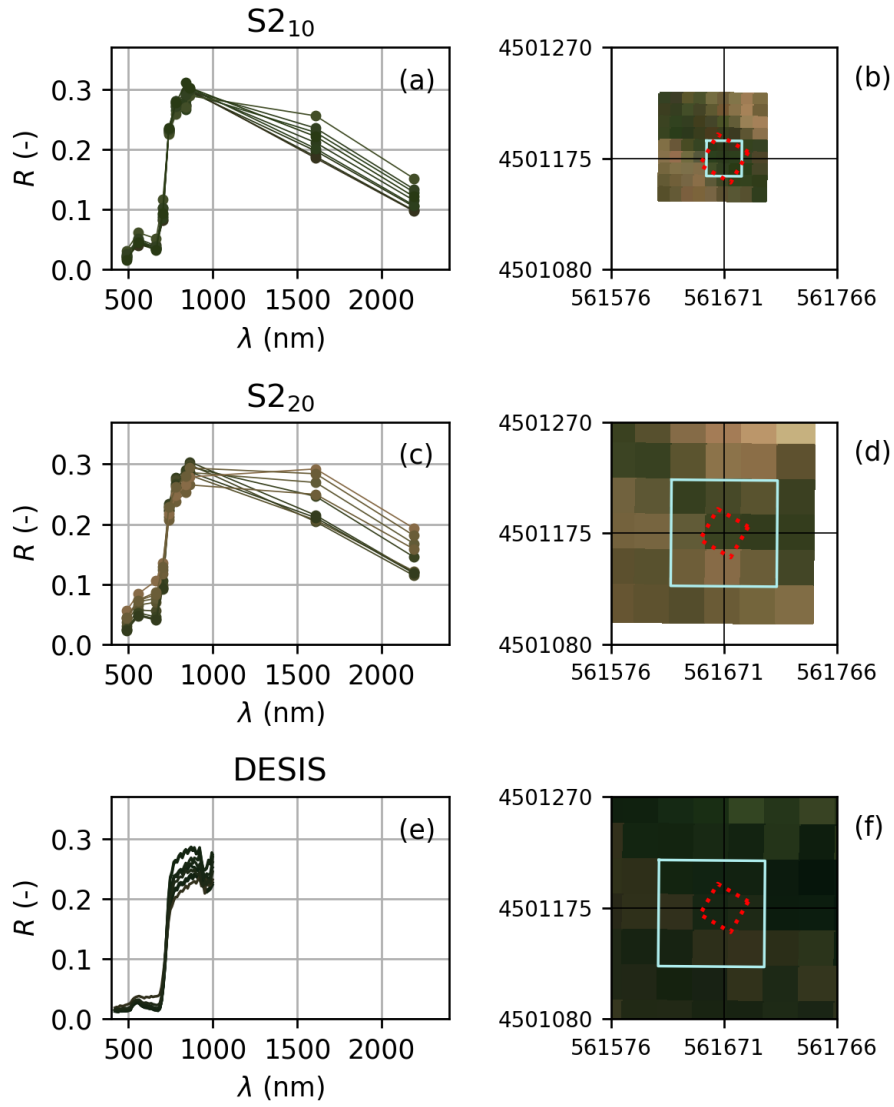


Figure 5. Example of the remote sensing data used in one of the FunDivEUROPE sites in Spain (SPA01). Spectra of the 3 x 3 pixels window used to compute the functional diversity metrics (first column) and red-green-blue composition of the clips around the site (second column) together with the plot (red dashed line) and the 3 x 3 pixels window (pale blue) used to compute functional diversity metrics. Sentinel-2 MSI @ 10 m pixel in 2015 (S2₁₀, first row), Sentinel-2 MSI @ 30 m pixel in 2015 (S2₃₀, second row) and DESIS @ 30 m pixel in 2020 (third row).

Spectra and imagery pixel colors are matched.

430 2.4.3 Optical traits retrieval and biodiversity metrics

431 FDMs were also computed from optical traits (T_{optical}) estimated from DESIS, S2₁₀, and S2₃₀
432 reflectance factors for all the pixels within the 3 x 3 window surrounding each plot. We used an approach
433 similar to the one described in section 2.3.4; however, in this case, we inverted the model (not the emulator)
434 in the second step to account for the off-nadir view angles and regularized the cost function (Supplementary
435 SM4). Next, we assessed the retrieval quality by comparing *LAI*, chlorophyll concentration ($\mu\text{g g}^{-1}$)
436 (computed from C_{ab} , and dry matter content (C_{dm}) estimates), and C_{dm} with field *LAI*, leaf N_{mass} , and C_{dm} ,
437 respectively. After the inversion, we computed the FDMs described in section 2.1 on the estimated optical
438 traits. As with the imagery, we gathered all the optical traits to provide a common standardization and PCA
439 models for dimensionality reduction and kept the components explaining at least 98% of the variance.

440 **3. RESULTS**

441 **3.1 Links between functional diversity metrics**

442 The comparison of FDMs computed from field plant traits (T_{RTM}) and reflectance factors (R) under
443 ideal conditions (noiseless, full-hyperspectral, and maximum spatial resolution) at the global scale (all data
444 simultaneously) showed that $RaoQ_{\alpha=1}$ (Fig. 6g) presents the highest R^2 , followed by $FDis$ (Fig. 6d) and
445 $RaoQ_{\alpha=2}$ (Fig. 6h), and then $RaoQ$ (Fig. 6e), $FRic$ (Fig. 6a) and $RaoQ_{\alpha=\infty}$ (Fig. 6i). The strength of the
446 relationships of the parametric $RaoQ$ (Rocchini et al. 2021) decreased with the value of α (not shown). For
447 $\alpha = 0$, extreme values strongly reduced the coherence of the relationship. $FDiv$ (Fig. 6c) and especially
448 $FEve$ (Fig. 6b) showed weak relationships. Results at the global scale were coherent with those found at
449 the local scale (1000 comparisons, one per species' pool); median values of R^2 (and $NRMSE$) were always
450 larger than those found at the global scale (e.g., 0.75 vs. 0.89 R^2 for $RaoQ_{\alpha=1}$). However, the performance
451 at the local scale featured large variability. The 2.5 % percentile of the R^2 distribution was below 0.35 in
452 most of the metrics, except for $RaoQ_{\alpha=1}$ and $FRic$. Most FDMs reached very high R^2 (~ 0.98) locally, except

453 *FDiv* and *FEve*, whose maximum (97.5 % percentile) values are 0.64 and 0.62, respectively. Still, median
 454 values were low for these FDMs, suggesting that vegetation evenness and divergence could not be reliably
 455 inferred from imagery using these metrics at local scales.

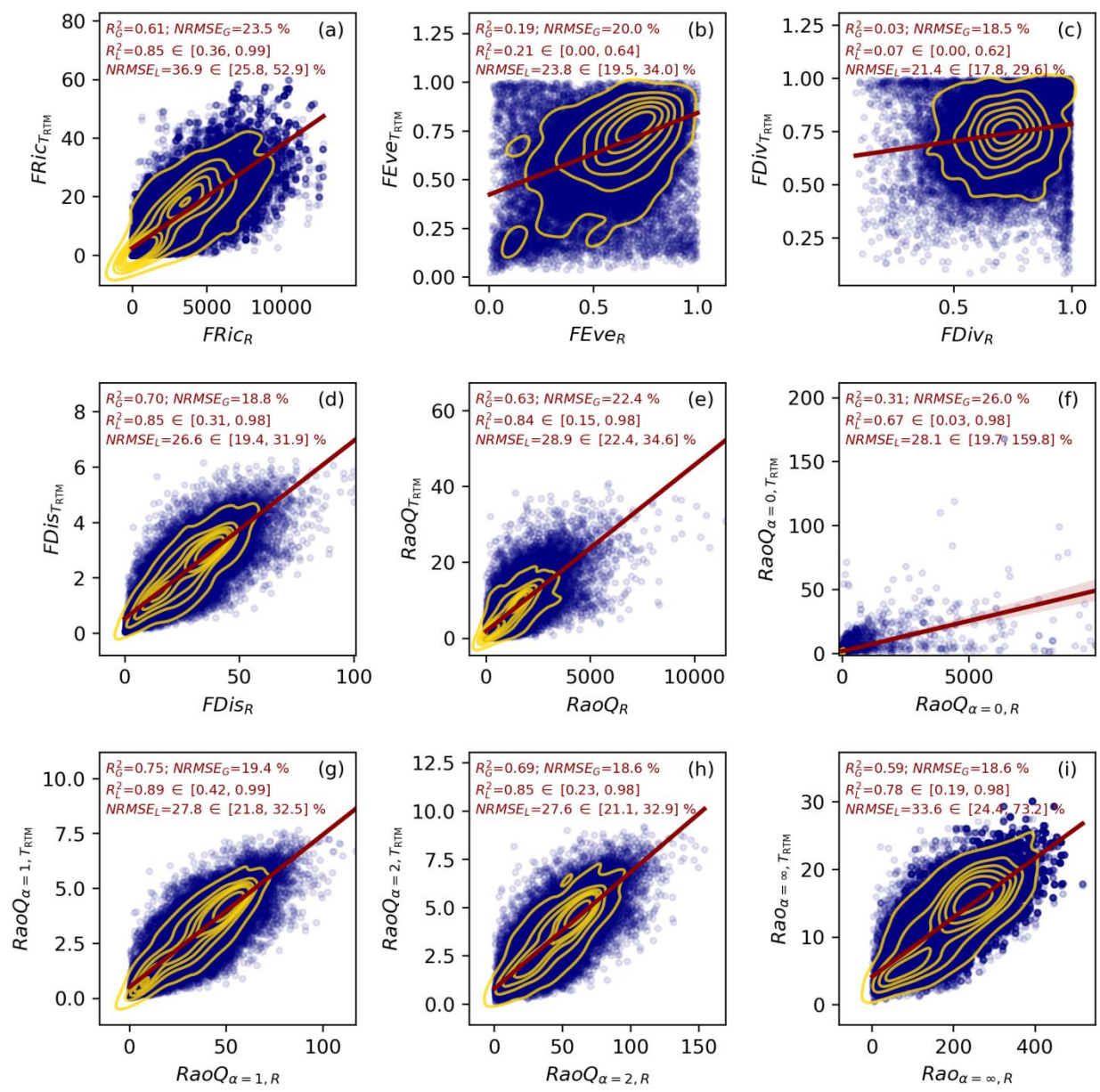


Figure 6. Relationship between the functional diversity metrics computed from the reflectance (subscript “R”) factors and field plant traits (subscript “TRTM”) using the *dbFD* package (a-e) or the parametric Rao’s *Q* formulation with different values of the parameter α (f-i). Regression lines summarize the comparison at the global scale; the

shaded areas around the regression lines represent the 95 % confidence interval of the line. Each subplot includes the statistics of the relationship at the global scale (on top, subscript “G”) and the median and 95 % confidence interval of the statistics at the local scale (below, subscript “L”).

456

457 The comparison of FDMs computed from field plant traits (T_{RTM}) and estimated optical traits
458 (T_{optical}) under ideal conditions (Fig. 7) led to results similar to those obtained with the reflectance factors
459 (Fig. 6). However, this time FDMs’ performance was higher in almost all the cases, both at the global and
460 the local scales (median values). Higher correlations occurred despite the uncertainties in the retrieval (Fig.
461 S1) and the fact that FDMs were computed from a subset of the optical traits controlling R (Supplementary
462 SM2). T_{optical} were retrieved with different degrees of success. Evaluated against the field plant traits, the
463 estimates of LAI and $LIDF_a$ (Fig. S1j,h, respectively) showed biases but high R^2 values. C_{ab} , C_{dm} , and C_w
464 (Fig. S1b,f,g, respectively) were acceptably retrieved with frequent overestimation for low values. The leaf
465 parameter N (Fig. S1a) was often underestimated, $LIDF_b$ (Fig. S1i) was weakly constrained, whereas C_s
466 and C_{ant} (Fig. S1d,e) were consistently underestimated. The retrieval performance was slightly better when
467 evaluated at local scales (median of the statistics); however, there was a large dispersion of R^2 , whose lowest
468 values were close to 0.0 in all the cases. The retrievals worsened as the remote sensing resolutions decreased
469 and the noise increased (Table S3). Results were slightly better when the model error was minimized using
470 the same emulator for simulation and inversion, both in the retrieval (Fig. S2) and the relationships between
471 FDMs (Fig. S3). This analysis proved that model error (Table S2) influences the estimation of plant
472 functional diversity with the optical trait estimation approach.

473

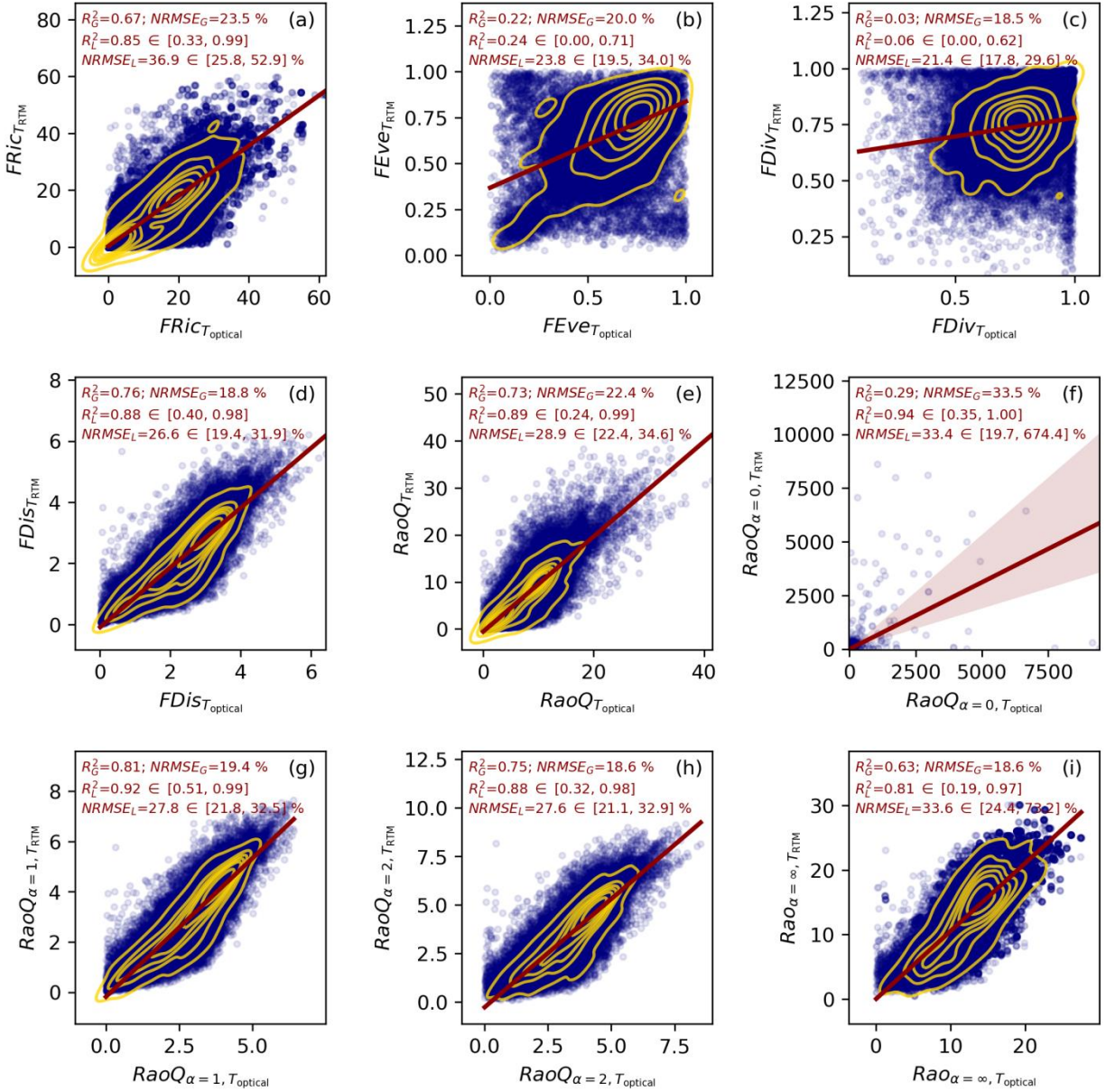


Figure 7. Relationship between the functional diversity metrics computed from optical traits estimated via radiative transfer model inversion (subscript “ T_{optical} ”) and field plant traits (subscript “ T_{RTM} ”) using the *dbFD* package (a-e), or the parametric Rao’s Q formulation with different values of the parameter α (f-i). Two different emulators simulated the reflectance factors and estimated the optical traits to induce model error. Regression lines summarize the comparison at the global scale; the shaded areas around the regression lines represent the 95 % confidence interval of the line. Each subplot includes the statistics of the relationship at the global scale (on top, subscript “G”) and the median and 95 % confidence interval of the statistics at the local scale (below, subscript “L”).

474

475 The relationships between field (T_{RTM}) and remote sensing-based (R or T_{optical}) FDMs depended on
476 the remote sensing features (spatial, spectral, and signal noise) and the way the metrics were compared
477 (scale and spatial mismatch). The joint analysis of all these factors (Fig. 8) confirmed that 1) $RaoQ$, $FDis$,
478 and to a lesser extent $FRic$, allow the estimation of plant functional diversity from remote sensing. 2) Local-
479 scale relationships (Fig. 8e-h) were stronger on average than global relationships (Fig. 8a-d) ($\tilde{R}_L^2 > R_G^2$).
480 The analysis also led to three additional discoveries: 1) Spatial resolution loss is the most relevant factor
481 reducing the correlation between remote sensing metrics and field metrics in all the cases (differences in
482 marker colors); whereas the effect of spectral configuration and noise depends on the approach used to
483 compute FDMs (reflectance or optical traits). Noise and spectral configuration had little effect when field
484 FDMs at maximum spatial resolution were compared with R -based metrics at sensor resolution (hi-res, Fig.
485 8a,e, and Table S4). However, these became more important when the metrics were computed from optical
486 traits (hi-res, Fig. 8c,g and Table S5). Then, in the absence of noise (brightest tones, smallest markers), R^2
487 was larger than for the reflectance-based approach (Fig. 8a,e), and differences between sensors (marker
488 shape) were small at all the spatial resolutions. However, except for the Full-hyperspectral configuration,
489 R^2 decreased as noise increased (larger and darker markers), making the correlations weaker than for the
490 reflectance-based FDMs. Still, when no species could be discriminated ($S_{\text{res},0}$) noise and spectral features
491 lost most influence, and R^2 was low in all cases. 2) When remote sensing estimates were compared with
492 field data integrated at the sensor spatial resolution (RS-res, mimicking the image pixels), the relationships
493 were more robust to the spatial resolution loss. Moreover, metrics computed from reflectance factors (Fig.
494 8b,f and Table S6) were more robust than those computed from retrieved optical traits (RS-res, Fig. 8d,h,
495 and Table S7 vs. Fig. 8c,g). 3) For both approaches (reflectance or optical trait-based metrics), matching
496 field and remote sensing resolutions (RS-res, Fig. 8b,d,f,h) led to spurious R^2 increases for $FRic$, $FEve$, and
497 $FDiv$; induced by noise or spatial resolution loss.

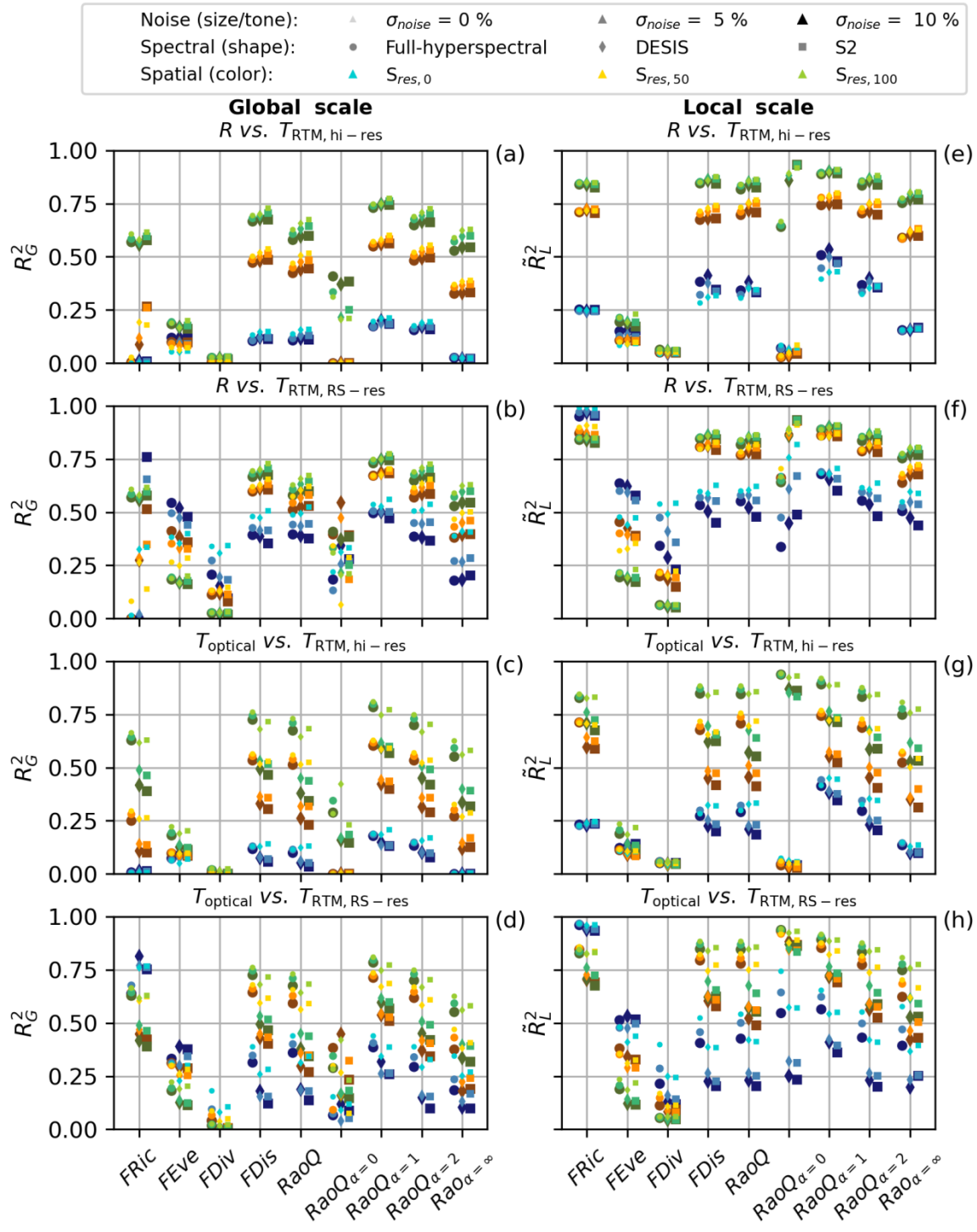


Figure 8. Evaluation of remote sensing features on the relationships between functional diversity metrics. Metrics computed from field plant traits (T_{RTM}) are compared with remote sensing metrics computed either from reflectance factors (R) or estimated optical traits ($T_{optical}$). The left column presents R^2 of the relationships between metrics

compared at the global scale (R_G^2), the right column shows the median R^2 of the evaluation at the local scale (\tilde{R}_L^2). Functional diversity metrics computed from reflectance factors at sensor resolution are compared with field metrics at maximum spatial resolution (hi-res), representing the mismatch between remote sensors and field surveys (a, e) and remote sensing resolution (RS-res) mimicking remote sensing-oriented field surveys (b, f). Functional diversity metrics computed from estimated optical traits at sensor resolution are compared with field metrics at maximum spatial resolution (hi-res) (c, g) and remote sensing resolution (RS-res) (d, h). Markers show different spectral configurations; color ranges indicate spatial resolution, whereas marker size and tone represent noise level.

498

499 **3.2 DESIS and Sentinel-2 imagery over FunDivEUROPE sites**

500 As in the simulations, optical traits retrieval from RS was not exempt from uncertainty. Still, the
501 evaluation against field traits (Fig. S4, subscript “F”) suggests that, at least for key traits, such as LAI , C_{ab} ,
502 and C_{dm} , the retrieval results were reasonable and within the expected performances (Table S3), or at least
503 similar for all the RS datasets. $NRMSE$ ranged between 21 and 37 % for the three variables, whereas R^2
504 showed larger variability (from 0.00 to 0.93). The retrieval of LAI (Fig. S4a,d,g) was most problematic in
505 Romania, still taking both countries together (All), R^2 was high ($R^2 \geq 0.92$ for Sentinel-2, $R^2 = 0.65$ for
506 DESIS). Chlorophyll concentration (per unit mass) showed positive relationships with field N_{mass} (Fig.
507 S4b,e,h). Coherently with the simulations (Table S3), the retrievals’ performance generally increased with
508 spatial resolution. In the case of DESIS, the lower R^2 might relate to larger uncertainties in LAI and C_{dm}
509 retrieval. C_{dm} was overestimated, especially for DESIS in Spain (Fig. S4c,f,i), but the correlations were
510 moderately strong for the whole dataset (R^2 between 0.47 and 0.54). The fact that DESIS does not cover
511 the short wave infrared might explain this bias, which agrees with the performances found in the simulations
512 (Table S3). Retrieval performances were similar or even higher for Sentinel-2 in 2020 (Fig. S5).

513 The comparison of FDMs computed from satellite imagery and field plant traits sampled in the
514 FunDivEUROPE plots led to metric and sensor-dependent results (Fig. 9). These were evaluated with the
515 Pearson correlation coefficient (r_{Pearson}) to identify negative correlations. $FEve$ and $FDiv$ were never

516 significantly correlated, and *FRic* only weakly once. $S2_{10}$ showed significant positive correlations between
517 field taxonomic and functional diversity metrics for most of the remaining FDMs. *R*-based metrics (Fig.
518 9a,d) were more significantly and more often correlated than those calculated from optical traits (Fig. 9g,j)
519 except with the taxonomical field metrics (species richness *S* and Shannon index *H*). DESIS only achieved
520 a significant correlation between *FDis* computed from reflectance factors and field species richness (Fig.
521 9c). Also, weak significant correlations were found between field and optical trait metrics with field
522 $RaoQ_{\alpha=0}$ when Sentinel-2 was resampled to DESIS spatial resolution ($S2_{30}$) (Fig. 9k). Nonetheless,
523 simulations showed that $RaoQ_{\alpha=0}$ was prone to extreme values that might inflate correlations in small
524 datasets. The fact that only $RaoQ_{\alpha=0}$ correlates and no others such as $RaoQ_{\alpha=1}$ or *FDis* suggest these results
525 could be spurious. Despite the significance, the relationships found for $S2_{10}$ were relatively weak. The
526 maximum R^2 found in significant correlations for each group of FDMs evaluated were 0.27 (Fig. 9a), 0.30
527 (Fig. 9d), 0.18 (Fig. 9g), and 0.18 (Fig. 9j). For DESIS and $S2_{30}$, the maximum significant R^2 were 0.20
528 (Fig. 9c) and 0.09 (Fig. 9k), respectively. Overall results were similar but weaker for Sentinel-2 imagery in
529 2020 (Fig. S6). FDMs computed from optical traits did not achieve significant correlations in this case.
530

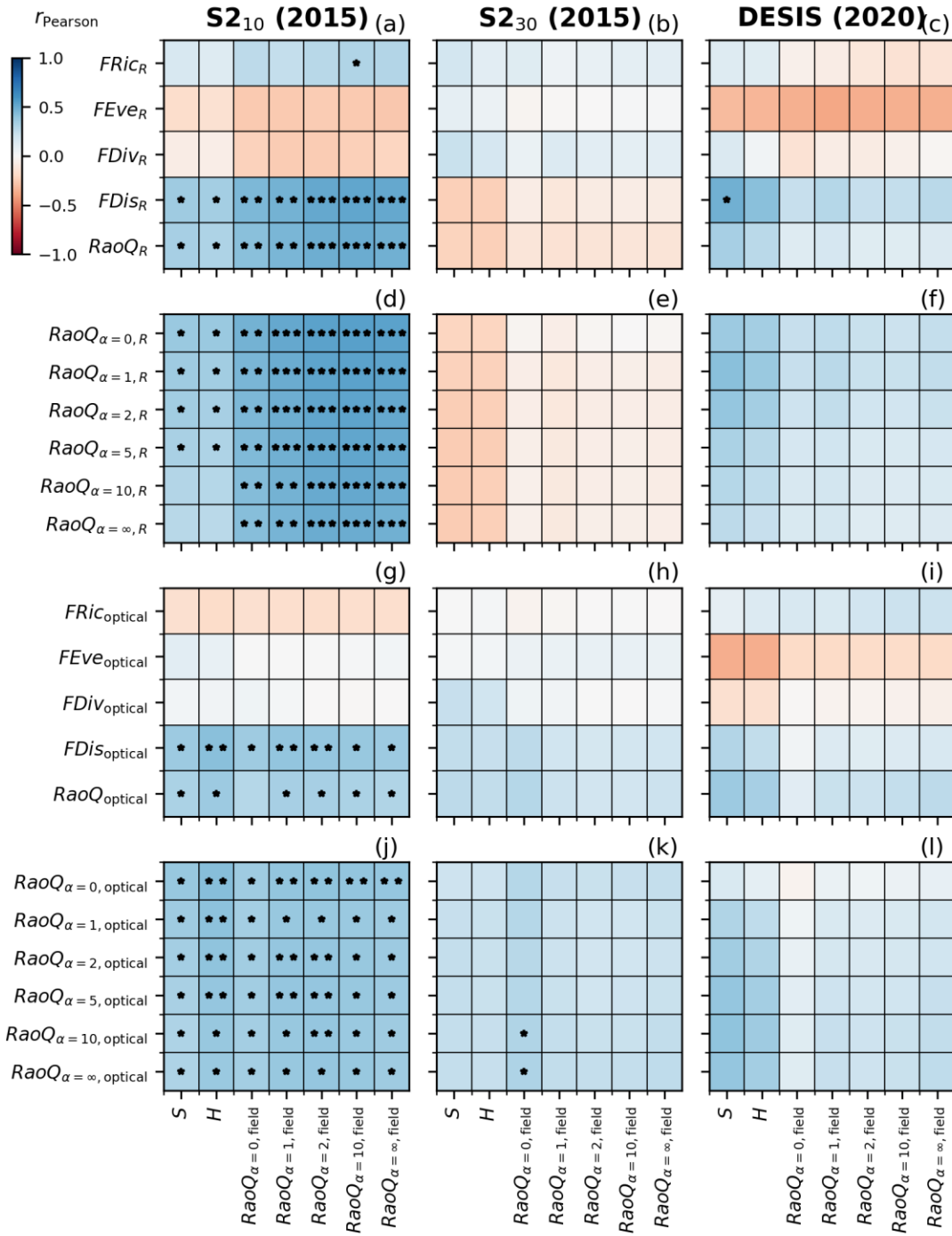


Figure 9. Pearson correlation coefficient between taxonomical and functional diversity metrics computed from field plant traits (subscript “field”, x -axis) and functional diversity metrics computed from remote sensing information (y -axis): the reflectance factors (subscript “R”, first two rows) or the optical traits (subscript “optical”, last two rows).

In each case, the *dbFD* package metrics are presented first, and the parametric Rao's Q afterward. The statistics correspond to Sentinel-2 MSI @ 10 m spatial resolution ($S2_{10}$, first column), Sentinel-2 MSI @ 30 m spatial resolution ($S2_{30}$, second column), and DESIS at 30 m spatial resolution (DESI, third column). Sentinel-2 imagery was acquired in 2015. Asterisks indicate the significance of the correlation (two-tailed) according to its p-value (p):

*** $\rightarrow p < 0.001$, ** $\rightarrow 0.001 \leq p < 0.01$, and * $\rightarrow 0.01 \leq p < 0.05$.

531

532 4. DISCUSSION

533 4.1 Can we infer functional diversity from space?

534 Our simulations demonstrate that the SVH is valid for some aspects of functional diversity, but not
535 all of them. Metrics based on the dispersion (Rao's Q formulations, $FDis$) and, to a lesser extent, range
536 ($FRic$) can provide robust insight into plant functional diversity from RS data. However, the metrics related
537 to evenness and divergence failed to connect spectral and plant functional diversities. To our knowledge,
538 this is the first study that evaluates these links mechanistically and in a generalizable way. Previous studies
539 also addressed specific questions supporting modeling with local data only, covering a limited range of
540 traits, combinations of species, and sensors (Fassnacht et al. 2022; Hauser et al. 2021b; Heumann et al.
541 2015; Laliberté et al. 2020; Wang et al. 2018b). Our simulations also demonstrate that plant functional
542 diversity can be inferred from optical traits with even higher precision despite the inherent uncertainties of
543 the retrieval. This fact might be explained by the RTM removing the non-linearity between field plant traits
544 and canopy reflectance and the contribution of other elements such as soil.

545 The potential of Rao's Q and $FDis$ metrics to connect plant functional and spectral diversity might
546 rely on the fact that they account both for relative abundances and the ranges of the traits in the
547 multidimensional space. We hypothesize that these metrics would be little affected by equifinal estimates
548 of optical traits as long as these exchange their variability while keeping the diversity information in the
549 overall set of traits evaluated. Hauser et al. (2021a) also found good correlations with field FDMs using this

550 approach. *FRic* showed lower performance and robustness than the dispersion metrics, likely since it does
551 not account for the relative abundance of species. Moreover, since *FRic* is the trait's convex hull volume,
552 it is potentially sensitive to extreme values. *FRic* presents a strong sensitivity to the degradation of spatial
553 resolution (Fig. 8a,c,e,g) but shows much stronger correlations (even spuriously increased) when field data
554 are compared at the spatial resolution of the sensor at local scales (Fig. 8f,h). These results are consistent
555 with the convex-hull-based metric's better performance than Rao's Q reported by Hauser et al. (2021b). In
556 all cases, dimensionality reduction might contribute to the robustness against noise and other uncertainties.
557 However, noise might as well compensate for the loss of variability induced by degraded spatial resolution
558 (Fig. 4b,e,h), spuriously increasing the strength of the relationships between some of the FDMs (Fig. 8).

559 The large scattering observed in the relationships between the indices of evenness and divergence
560 computed from remote sensing and field plant variables might be related to the fact that these metrics look
561 at the dispersion of species within the convex-hull formed by their traits but ignore its volume (Laliberté
562 and Legendre 2010). Combined with the non-linear nature of the relationships between reflectance and field
563 plant traits, this fact might allow for situations where intermediate values of field *FEve* or *FDiv* lead to
564 extreme values of the RS-based metrics and *vice versa*. *FEve* is the metric the least correlated with *FDis*
565 and Rao's Q (Laliberté and Legendre 2010), and when compared, RS and field values are widely scattered
566 (Fig 5b and 6b). *FDiv* is more related by construction to *FDis* but presents numerous cases where one of
567 the metrics (from RS or field) takes an extreme value (close to 0 or 1), independently of the other (Fig. 6c
568 and 7c). Ignoring the convex-hull volume might make these metrics less robust to uncertainty and
569 equifinality of the optical traits, leading to spurious correlation increases when metrics are compared at
570 sensor resolution (Fig. 8b,d,f,h).

571

572 **4.2 Are plant diversity indices comparable beyond a single image or ecosystem?**

573 Especially for Rao's Q , $FDis$, and $FRic$, the relationships between RS and vegetation functional
574 diversity are robust at global (e.g., between ecosystems or images) and local (a smaller region or a single
575 image) scales. However, even if median R^2 is larger at the local scale, the large variability of performances
576 registered (Table S4-S7) recommends caution when interpreting RS estimates locally or within a limited
577 number of ecosystems. This performance's variability implies that moderate correlations might be found
578 for $FEve$ and $FDiv$ in local studies allowing for plausible interpretation of their patterns with the known
579 ecological features of the study site (e.g., Schneider et al. (2017)). However, our results suggest that these
580 metrics should not be trusted since R^2 is prone to be inflated by noise and spatial resolution degradation
581 (Fig. 8). More research is needed to understand the control of specific plant traits on the relationships
582 between functional and spectral diversity and the situations where the metrics are most prone to fail or
583 succeed. For example, Rocchini et al. (2021) suggested that the mixture of crops and urban areas spuriously
584 inflated spectral variability. In our simulations, 11.89 % of the species featured $LAI < 1.0$, which might have
585 produced similar effects. When possible, misleading information should be removed from the spectral
586 datasets to ensure that the spectral variability is only driven by plant diversity. For example, Gholizadeh et
587 al. (2018) and Laliberté et al. (2020) proposed to classify and mask non-vegetated pixels (soil and shades,
588 respectively) before remote characterization of taxonomic and functional plant diversity. In this regard, the
589 inversion of RTMs might contribute to separating background effects from vegetation properties since both
590 are represented.

591 Interestingly, Rao's Q , $FDis$, and $FRic$ are comparable between different ecosystems/images
592 despite not sharing a common standardization (and dimensionality reduction). Botta-Dukát (2005) indicated
593 that the same standardization should be applied to the whole dataset when comparing different
594 communities. However, this approach is unsuitable for operational remote sensing since RS products cannot
595 be reprocessed every time a new image is added to the dataset. Botta-Dukát (2005) proposed scaling within
596 plausible trait ranges as an alternative to this standardization. However, his study did not consider a
597 posterior dimensionality reduction, where standardization could be advantageous (van den Berg et al. 2006).

598 Whether or not global RS products of plant functional diversity require a common
599 standardization/dimensionality reduction model needs to be solved before these can be implemented. We
600 tried to apply a common standardization and PCA model to all the data simulations to explore the possibility
601 of using default models to all RS imagery of a mission. These models were not produced from the
602 simulation used to compute FDMs but from an independent simulation of 10,000 species. The approach
603 failed to improve the performance of the parametric Rao's Q metrics, with the R^2 falling below 0.25 at the
604 global scale (not shown). Our simulations show that applying image-based standardization and PCA still
605 allows the comparison of FDMs between different regions or images. Therefore, this approach should also
606 be suitable for analyzing time series and the development of global RS products. Nonetheless, the
607 correlations are weaker than at the local scale (in average). Therefore, alternative methods improving the
608 precision and spatio-temporal consistency of future global plant diversity maps should be explored.

609

610 **4.3 What are the limitations and ways forward?**

611 Our simulations reveal that spatial resolution, defined as the capability to resolve or identify the
612 spectral properties of individual species, plays the most relevant role in the ability of RS to infer plant
613 functional diversity. In an RS validation framework, the decrease of spatial resolution produces specie's
614 spectra and abundances that do not correspond with those measured in the field and, therefore, a discrepancy
615 between the FDMs compared. Moreover, as the pixel size increases, it includes new species and trait values
616 not present in the field plots used as a reference for RS (e.g., results in section 3.2). New species could also
617 be introduced by the spatial mismatch between RS pixels and field plots. We compared field FDMs with
618 the RS estimates simulating this mismatch and found that the degradation of spatial resolution strongly
619 reduced the performance of RS to infer functional diversity (Fig. 8a,c,e,g). We also compared both data at
620 the RS scale, trying to reproduce what is observed by the sensor from field data. Spatial matching reduced
621 performance loss, but it was still considerable when none of the species could be identified (Fig. 8b,f,d,h).

622 In addition, we proved that model error influences optical traits retrieval (Fig. S1 vs. Fig. S2) and the
623 subsequent estimation of functional diversity (Fig. 7 vs. Fig. S3). Therefore, a careful selection of the RTM
624 to best represent the canopy monitored could benefit this approach.

625 Surprisingly, sensor spectral configuration plays a minor role when FDMs are directly computed
626 from R . Likely, dimensionality reduction lessens the differences between the information present in datasets
627 of different spectral features. However, this can also be understood as a need for metrics capable of
628 optimally extracting functional diversity information from hyperspectral data. Still, notice that
629 standardization and removal of variables covariance is necessary; simulations avoiding these steps led to
630 weak correlations between FDMs (not shown). Nonetheless, sensor spectral features were more influential
631 when FDMs were computed from optical traits; which suggests that hyperspectral missions (e.g.,
632 Environmental Mapping and Analysis Program (EnMAP), DESIS, PRecurso IperSpettrale della Missione
633 Applicativa (PRISMA), Copernicus Hyperspectral Imaging Mission (CHIME), Surface Biology and
634 Geology (SBG)) should be preferred for this approach. Furthermore, simulations show that reducing sensor
635 spectral range or resolution makes this approach more sensitive to noise and spatial resolution decrease
636 (Fig. 8c,d,g,h).

637 Analyzing the impact of different remote sensing features clarified the limits and possibilities of
638 different mission concepts to infer plant functional diversity from space. When the spatial resolution is
639 prioritized, FDMs based on R directly are most likely to succeed. When the spectral resolution is higher
640 (e.g., hyperspectral imagers), the approaches based on optical traits would be advantageous under two
641 conditions: low noise and accepting that trait variability is assessed between small communities of
642 vegetation (pixels), not individual species. In all the cases, both approaches might be used together to
643 evaluate the robustness/reliability of the estimates. Ideally, a biodiversity monitoring system would benefit
644 from combining mid-spatial-resolution hyperspectral imagers (e.g., EnMAP, DESIS, PRISMA, CHIME,
645 SBG, etc.) with high-spatial-resolution multispectral sensors (e.g., Sentinel-2); potentially also sharpening

646 or down-scaling the hyperspectral data. This combination could provide redundant (and thus more robust)
647 estimates of plant functional diversity, exploiting each mission concept's best features.

648 Our results are robust to simulation design. For example, simulations not constraining the
649 plausibility of the relationships between leaf traits led to similar results and the same conclusions (not
650 shown). Additional challenges not addressed in this work could increase the uncertainty of the relationships
651 explored. Still, they could be analyzed in the future using a modeling framework like the one described
652 here. For example, our simulations ignored intra-specific functional variability. It could complicate species
653 classification from remote sensing and lead to divergences between taxonomic and functional diversities.
654 However, from a remote sensing perspective, two pixels can be considered different species, being the
655 degree of functional diversity determined by their dissimilarity and not their taxonomic classification. We
656 hypothesize that intra-specific variability might be the least problematic when RS and field data are
657 compared at the same spatial resolution. An additional challenge would be assessing nearby species
658 functionally different with similar spectral properties. Also, using a unidimensional RTM might not be
659 representative of canopies with a strong geometrical scattering component. The effects of canopy geometry
660 could be further analyzed with three-dimensional RTMs. We did not consider either the vertical overlap of
661 species, which reduces the contribution of the shortest plants to the RS signal. However, these plants might
662 be sampled in field surveys, leading to mismatches between ground and remote estimates of plant functional
663 diversity. In this regard, active RS using radar or lidar could offer additional information on the vertical
664 distribution of vegetation and the variability of plants in the understory and characterize vegetation
665 (structural) properties (Asner et al. 2017; Bae et al. 2019; Ma et al. 2020; Simonson et al. 2014; Valbuena
666 et al. 2020). However, active RS would also be the subject of the issues related to spatial resolution and
667 noise. Spaceborne radar missions such as Sentinel-1 (Torres et al. 2012) can today provide global coverage
668 with pixel sizes close to the size of tree crowns. However, the complexity of the SAR backscatter, the
669 enlarged footprint from oblique observation, and signal noise might limit the discrimination of individual
670 trees (Bae et al. 2019). Still, radar information could be valuable, providing information regarding the

671 understory and soil water content, which could relate to the distribution of species governing the top of the
672 canopy (Fauvel et al. 2020). Spaceborne lidar does not yet offer comparable coverage and resolutions. Still,
673 with a footprint of 25 m, Global Ecosystem Dynamics Investigation (GEDI) mission (Coyle et al. 2015)
674 could provide valuable information on the vertical distribution of vegetation that could be enhanced when
675 combined with optical or radar data (Valbuena et al. 2020). Beyond global coverage products, our
676 simulations suggest that the airborne and drone-borne platforms would offer the best possibilities to infer
677 functional diversity remotely. Especially the airborne systems allow the combination of active and passive
678 sensors featuring high spatial resolutions (Adhikari et al. 2020; Almeida et al. 2021; Asner et al. 2017;
679 Schneider et al. 2017; Zhao et al. 2018), and including visible and near-infrared (Gholizadeh et al. 2019;
680 Melville et al. 2019) and short-wave infrared hyperspectral configurations (Asner et al. 2015; Jetz et al.
681 2016). Furthermore, they can carry sensors to map other signals intimately linked to plant function, such as
682 chlorophyll sun-induced fluorescence (Tagliabue et al. 2020). Nowadays, these sensors are the most suitable
683 for detailed surveillance of valuable and endangered areas or the generation of high-quality datasets that
684 enable the development or evaluation of methods to be later applied to satellite imagery.

685

686 **4.4 Applied optical remote sensing of plant functional diversity: a case study on the forests of the** 687 **FunDivEUROPE Network**

688 The comparison between field estimates of functional diversity in forests and RS imagery from
689 Sentinel-2 and DESIS sensors was consistent with the conclusions drawn from the simulations. The best-
690 performing metrics in the simulations Rao's Q and $FDis$ provided significant correlations in the study case
691 most of the time. However, Sentinel-2 and DESIS performances were very different. Only $S2_{10}$ provided
692 several significant correlations with field FDMs (weak, $R^2 \leq 0.30$, but coherent with simulations, e.g., Fig.
693 8). This analysis does not seek to assess the missions' potential to estimate plant functional diversity since
694 none of them can, for example, identify the species of the field plots and are therefore suboptimal for such

695 evaluation. The value of this exercise is the coherence found between our simulation framework and
696 observations. A potential reason for DESIS lower performance might be the larger mismatch between the
697 acquisition of DESIS and field data (7 years). We minimized the effect of this temporal gap by limiting the
698 analysis of DESIS to plots stable between 2015 and 2020. Sentinel-2 imagery acquired in 2015 and 2020
699 provided similar results. Still, the strength of the correlations decreased in 2020, and these were not
700 significant for the metrics computed from the optical traits (Fig. S9 vs. S6) despite some being closer to
701 field data in 2020 (Fig. S4 vs. S5). Thus, the temporal gap might account for part of the differences between
702 DESIS and Sentinel-2. However, the lack of significant correlations of Sentinel-2 resampled at 30 m
703 suggests that the coarser spatial resolution of DESIS (equal to field plot size) and not the temporal mismatch
704 was the main limitation for comparing field and RS estimates of plant diversity. Still, unlike in the
705 simulations, we could not disentangle the contribution of the different sources of uncertainty and
706 mismatches when comparing this imagery.

707 Our results agree with the fact that 10 m spatial resolution is enough to characterize the internal
708 variability of the plots. However, it was insufficient to discriminate the individual species and thus
709 suboptimal for estimating functional diversity. The correlations between FDMs were stronger for
710 reflectance (Fig. 9a,d) than for optical trait-based metrics (Fig. 9g,j), which agrees with the stronger
711 sensitivity of this method to noise and spectral configuration found in the simulations (Fig. 8c,d). The spatial
712 mismatch between plots and RS pixels might have added additional uncertainty. However, the 10 m buffer
713 of similar forest type, structure, and composition kept around the plots to minimize border effects should
714 minimize this uncertainty for $S_{2_{10}}$. Looking at the taxonomical metrics, $S_{2_{10}}$ found significant correlations
715 with species richness S and more strongly with the Shannon index H . DESIS found a weak but significant
716 relationship between FD_{is} and S ; whereas $S_{2_{30}}$ still found weak significant correlations for $RaoQ_{\alpha=0}$, which
717 simulations suggest might be spurious. Within the field metrics, H positively correlated with S ($R^2 = 0.47$),
718 and $RaoQ_{\alpha=1}$ with H ($R^2 = 0.96$) and S ($R^2 = 0.64$). The correlation between functional and taxonomic
719 diversity seems to be also captured by $S_{2_{10}}$ but not by $S_{2_{30}}$. In the case of DESIS, FD_{is} correlation with

720 field S might result from the richer spectral resolution capturing distinctive features of individual species,
721 even if these could be individually recognized. Nonetheless, as shown in the simulations, these results are
722 in part dependent on the spatial mismatch between field and RS data; in the case of DESIS and S2₃₀, stronger
723 correlations could be found if evaluated at their spatial resolution. The development of RS of biodiversity
724 products will benefit from establishing dedicated field plots, such as those proposed by Hauser et al.
725 (2021a), where vegetation is characterized in gridded plots that can be matched with pixels of RS imagers.

726 An additional challenge for RS of plant functional diversity is the conceptual gap between ecology
727 and RS regarding traits (Ustin and Gamon 2010). While the ecologists are interested in traits with
728 ecological, functional, and adaptative meaning, RS science is more interested or limited to properties that
729 significantly control light-vegetation interaction. This conceptual difference is not trivial. Hauser et al.
730 (2021a; 2021b) showed that accounting for the variability of structural traits such as LAI , which are not
731 considered functional traits, is necessary to explain spectral diversity. In our case, from the
732 FunDivEUROPE traits used to compute FDMs, only SLA (inversely related to leaf dry matter content, C_{dm}),
733 canopy height, and leaf area (related to leaf width) could be considered inputs of the most common
734 vegetation RTMs. This fact does not entirely prevent connecting RS signals with vegetation functional
735 diversity since some traits are shared or correlated (Kattenborn and Schmidtlein 2019). For example, C_{dm}
736 can relate inversely with SLA , C_{ab} with nitrogen and maximum carboxylation rate (Evans and Clarke 2019),
737 or LAI and canopy height with DBH in some cases (Fischer et al. 2019; Turner et al. 2000). However,
738 although global relationships between plant traits have been reported (Reich 2014; Wright et al. 2004), these
739 relationships can vary between species (Evans and Clarke 2019; Zhao et al. 2021). This variability in the
740 indirect connections between traits governing spectral diversity and the traits used by ecologists to quantify
741 functional diversity on the ground might obscure or prevent evaluating RS estimates of plant functional
742 diversity using ecological field data. This challenge was present when assessing RS estimates of functional
743 diversity in FunDivEUROPE since the field sampling was not designed for RS validation. We are aware
744 that part of the uncertainty found in the relationships evaluated might arise from this discrepancy, even

745 though we expect most field traits to correlate with RTM inputs. The remote sensing and ecology
746 communities should work together to design diversity experiments stretching gradients of traits that can be
747 remotely sensed, enabling the study of their relationship with function and development of remote sensing
748 maps of plant functional diversity.

749 **5. CONCLUSIONS**

750 In this work, we have systematically evaluated the links between spectral and functional diversity
751 and characterized the capability of remote sensing to provide accurate estimates of plant functional
752 diversity. Our modeling framework circumvented a lack of comprehensive data, allowing us to 1) identify
753 three functional diversity metrics (dispersion, richness, and Rao's Q) able to infer functional diversity
754 robustly from spectral diversity, 2) validate the use of both reflectance factors and optical traits estimated
755 via radiative transfer model inversion for these metrics, 3) determine that these metrics can deliver
756 summaries in different ecosystems and times and are therefore suitable for the generation of global remote
757 sensing products from the analysis of individual images, and 4) understand the effect of different remote
758 sensing features on the methods and metrics analyzed, learning that high spatial resolution imagers can rely
759 on reflectance factors despite the limited spectral information they provide, whereas hyperspectral imagers
760 with lower spatial resolution should infer plant diversity from optical traits. The case study results using
761 DESIS and Sentinel-2 imagery over FunDivEUROPE forest plots are coherent with the simulations.

762 Our approach clarifies some key issues, but further efforts are needed to generate field datasets
763 suitable for validating remote sensing estimates of plant functional diversity. Also, the gap between the
764 variables measured by biodiversity ecologists and those that can be remotely estimated (and therefore,
765 controlling the spectroradiometric signals) should be reduced to promote the development, evaluation, and
766 exploitation of such remote sensing products. The combination of new satellite missions overlapping
767 complementary resolutions and spectral information (e.g., hyperspectral, radar, lidar, high spatial resolution
768 imagery, etc.) could overcome some of the challenges found or not yet explored in this work.

770 ACKNOWLEDGEMENTS

771 JPL, MMi, and MMA acknowledge the German Aerospace Center (DLR) project OBEF-Accross2
772 "The Potential of Earth Observations to Capture Patterns of Biodiversity" (Contract No. 50EE1912,
773 German Aerospace Center). JPL, MMi, AH, CW, MMA, GK, FJB, and UW acknowledge the German
774 Aerospace Center (DLR) for providing DESIS imagery through the Announcement of Opportunity
775 "EBioIDEA: Enhancing Biodiversity Inventories with DESIS Imagery Analysis". FunDivEUROPE data
776 collection was supported by the European Union Seventh Framework Programme (FP7/2007-2013) (grant
777 agreement number: 265171) and the EU H2020 project Soil4Europe (Bioidversa 2017-2019). The in-situ
778 plant traits data collected over Romanian and Spanish sites were supported by a Marie-Curie Fellowship
779 (DIVERFOR, FP7-PEOPLE-2011-IEF. No. 302445) to R. Benavides. OB acknowledges funding from
780 project 10PFE/2021 Ministry of Research, Innovation and Digitalization within Program 1 - Development
781 of national research and development system, Subprogram 1.2 - Institutional Performance - RDI excellence
782 funding projects. XM was supported by the National Natural Science Foundation of China (42171305), the
783 Director Fund of the International Research Center of Big Data for Sustainable Development Goals
784 (CBAS2022DF006), and the Open Fund of State Key Laboratory of Remote Sensing Science
785 (OFSLRSS202229). We thank Prof. Dr. Michael Scherer-Lorenzen for coordinating the interaction with the
786 FunDivEUROPE network and Dr. Fernando Valladares for coordinating data production in
787 FunDivEUROPE sites in Spain. We thank Yuhan Li for helping collect and process Sentinel-2 data in 2020
788 for the verification task. ESA's Copernicus Open Access Hub enabled the free use of Sentinel-2 data.

789 APPENDIX A. VEGETATION TRAITS SIMULATION

790 We avoided unplausible combinations of field plant traits (i.e., T_{RTM}) and other inputs of the SCOPE
791 emulator during the definition of synthetic species combining three different approaches. First, we limited

792 the random sampling of these traits within realistic ranges (Table S1) commonly reported in the literature
793 (Bayat et al. 2018; Celesti et al. 2018; Feret et al. 2008; Houborg and Anderson 2009). Second, we avoided
794 unrealistic combinations of the leaf traits constraining N , C_{ab} , C_{ca} , C_{dm} , and C_w covariance with a Gaussian
795 Mixture Model (GMM). The GMM model was fit to the LOPEX (Hosgood et al. 1994) and ANGERS (Feret
796 et al. 2008) datasets using the expectation-maximization (EM) algorithm (Dempster et al. 1977)
797 implemented in the Python package *scikit-learn* (Pedregosa et al. 2011). We selected these databases since
798 they were produced to calibrate the coefficients of leaf RTMs and therefore present most of the traits needed,
799 including N . Notice that values of N are exclusively available in spectral libraries since this is a non-
800 measurable model parameter that can only be inferred via inversion of the leaf radiative transfer model.
801 Since N relates to the cellular arrangement inside the leaf, it can correlate with dry matter content, and it
802 has been shown to correlate with the specific leaf area (Jacquemoud and Baret 1990; Pacheco-Labrador et
803 al. 2021; Peters and Noble 2020). Third, we prevented the unrealistic co-existence of high chlorophyll (C_{ab})
804 with anthocyanins (C_{ant}) (Hughes et al. 2007) or senescent pigments (C_s) contents (Mattila et al. 2018) by
805 scaling the randomly sampled C_{ant} and C_s values by a factor ($f_{C,max}$) exponentially decreasing as a function
806 of C_{ab} as described in Eq. A.1:

$$f_{C,max} = e^{z \cdot \left(\frac{100 - C_{ab}}{100} - 1 \right)} \quad (\text{A.1})$$

808
809 $f_{C,max}$ ranges between 0 and 1, and z controls its decrease with C_{ab} . High C_s was strongly limited to
810 leaves featuring low C_{ab} ($z = 40$) since senescent pigments result from the degradation of chlorophylls and
811 other leaf constituents (Mattila et al. 2018; Pourcel et al. 2007). Anthocyanins were less strongly limited (z
812 = 7) since their functional role makes possible a positive correlation with C_{ab} in some cases (Gould 2004;
813 Hughes et al. 2007; Manetas 2006).

814 **APPENDIX B. SIMULATION OF SPECIES COMMUNITIES**

815 We produced 81 synthetic communities from each regional pool by sampling the species with
 816 varying relative abundances (A). Each pool contained a randomized number of species ($n_T \in [5, 30]$), of
 817 which n_s were similar and n_{ds} were dissimilar ($n_T = n_s + n_{ds}$). We labeled the species with an integer (n_{sp})
 818 ranging from 1 to n_T ; first the similar species ($n_{sp} \in [1, n_s]$) and then the dissimilar ones ($n_{sp} \in [n_s + 1, n_T]$)
 819 (Fig. B.1a). Then we produced relative species abundances for each community with a Gaussian distribution
 820 function whose mean (μ_{sp}) and standard deviation (σ_{sp}) were relative to species index space n_{sp} (Fig. B.1c).
 821 For each pool, we produced 81 communities from μ_{sp} and σ_{sp} gradients crossed in a 9×9 grid (Fig. B.1b).
 822 σ_{sp} ranged between 0.4 and 5.0 species, whereas μ_{sp} ranged between 0.2 and n_μ , where $n_\mu = n_s + f_{ds} \cdot n_{ds}$ and
 823 f_{ds} was a random value within the range $[0.2, 1.0]$. f_{ds} reduced the dominance of some of the dissimilar
 824 species in the regional communities, increasing their exoticism. Finally, the abundances of each community
 825 were normalized to add up to one. These synthetic communities presented different degrees of richness,
 826 evenness, and divergence (Villéger et al. 2008) and dominant species.

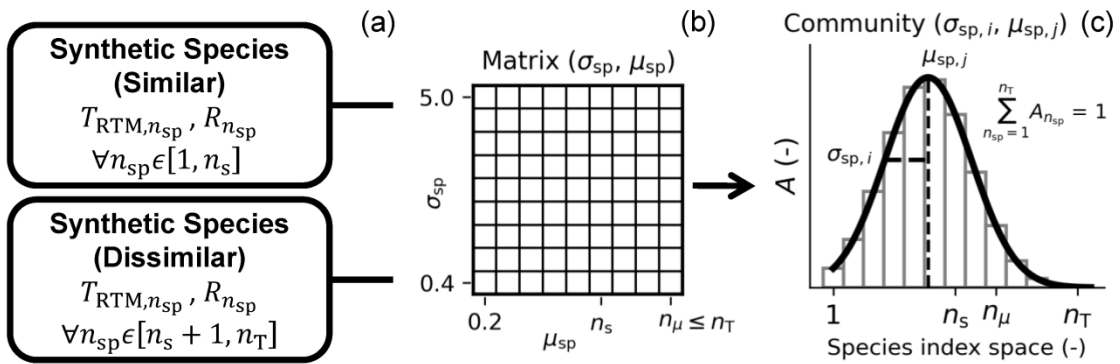


Figure B.1. Generation of several (81) synthetic communities from the same species pool. (a) Pool of n_s similar and n_{ds} dissimilar species adding up to n_T ; each species is labeled with an integer n_{sp} and characterized by a specific set of field plant traits (T_{RTM}) and the corresponding reflectance factor (R). (b) Communities matrix presenting the 81 combinations of the median (μ_{sp}) and the standard deviation (σ_{sp}) of the Gaussian distribution used to define the relative species abundance (A) of each community. i and j are row and column indices of the matrix; only a fraction

of the dissimilar species is allowed to dominate communities so that μ_{sp} ranges up to $n_{\mu} \leq n_T$. (c) Relative species abundance distribution of one of the communities.

827 APPENDIX C. DEGRADATION OF SPATIAL RESOLUTION

828 We simulated remote sensor spatial resolution degradation by mixing a fraction of the species
 829 within the community with each other (50 % or 100 % of the species). These mixtures represented the
 830 species observed by the remote sensor with a sub-optimal resolution, therefore, as a mixture. To do so, we
 831 generated a squared matrix (M) mapping the contribution of the original species (j columns) and to the
 832 species to be spatially degraded (i rows). The coefficients of the linear combination ($c_{i,j}$) were
 833 ($\sum_j c_{i,j} = 1, \forall i$). For the species that were not mixed, $c_{i,j} = 0 \forall i \neq j; c_{i,j} = 1 \forall i = j$. Fig. C.1 shows an
 834 example of this matrix for a community of 4 species where only species 1 and 2 are mixed.

835

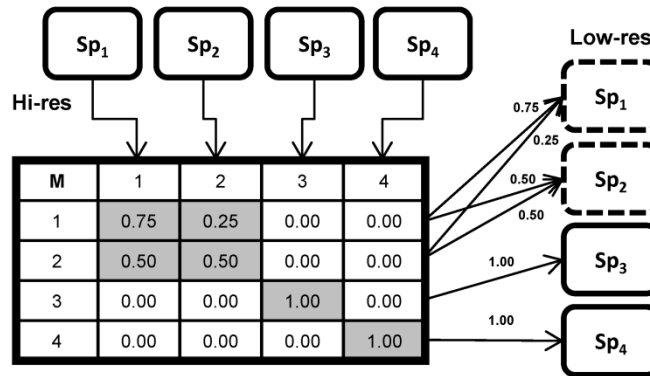


Figure C.1. Example of species mixture during spatial resolution degradation. Four species at high spatial resolution are observed from a sensor only able to distinguish two (solid lines); the rest are observed as a mixture (dashed lines). The table shows the coefficients of the mixture matrix M where columns represent the contribution of the original species to the degraded ones (rows). The procedure described is used to degrade the spatial resolution of reflectance factors, vegetation parameters, and relative abundances of the species of a regional pool.

836

837 Then, the reflectance factors, vegetation parameters, and abundances were mixed linearly,
838 combining the respective variables with the row coefficients of the matrix M:

839

$$X_{\text{low-Sres},i} = \sum_j (c_{i,j} X_{\text{hi-Sres},j}) \quad (\text{C.1})$$

840

841 where X represents any of the abovementioned variables, the subscripts “hi-Sres” and “low-Sres” stand for
842 high and low spatial resolution. The example of Fig. C.1 (first row) shows that what the remote sensor
843 would identify species 1 ($\text{Sp}_{1,\text{deg}}$) would be, in fact, a mixture 75% and 25% of the species 1 ($\text{Sp}_{1,\text{ori}}$) and 2
844 ($\text{Sp}_{2,\text{ori}}$), respectively. Relative abundances still had to be normalized after the combination to provide an
845 accumulated probability of 1 in each community. The mixture enabled the apparition of new species within
846 a community, which might happen when larger pixels sample a larger area outside the field plot used as a
847 reference (e.g., for field measurements or from a remote sensor with higher spatial resolution).

848 **REFERENCES**

- 849 Adhikari, H., Valbuena, R., Pellikka, P.K.E., & Heiskanen, J. (2020). Mapping forest structural
850 heterogeneity of tropical montane forest remnants from airborne laser scanning and Landsat time series.
851 *Ecological Indicators*, 108, 105739
- 852 Almeida, D.R.A.d., Broadbent, E.N., Ferreira, M.P., Meli, P., Zambrano, A.M.A., Gorgens, E.B., Resende,
853 A.F., de Almeida, C.T., do Amaral, C.H., Corte, A.P.D., Silva, C.A., Romanelli, J.P., Prata, G.A., de
854 Almeida Papa, D., Stark, S.C., Valbuena, R., Nelson, B.W., Guillemot, J., Féret, J.-B., Chazdon, R., &
855 Brancalion, P.H.S. (2021). Monitoring restored tropical forest diversity and structure through UAV-borne
856 hyperspectral and lidar fusion. *Remote Sensing of Environment*, 264, 112582
- 857 Alonso, K., Bachmann, M., Burch, K., Carmona, E., Cerra, D., de los Reyes, R., Dietrich, D., Heiden, U.,
858 Hölderlin, A., Ickes, J., Knodt, U., Krutz, D., Lester, H., Müller, R., Pagnutti, M., Reinartz, P., Richter, R.,
859 Ryan, R., Sebastian, I., & Tegler, M. (2019). Data Products, Quality and Validation of the DLR Earth
860 Sensing Imaging Spectrometer (DESI). *Sensors*, 19, 4471
- 861 Anderson, M.J. (2006). Distance-Based Tests for Homogeneity of Multivariate Dispersions. *Biometrics*,
862 62, 245-253
- 863 Asner, G.P., Martin, R.E., Anderson, C.B., & Knapp, D.E. (2015). Quantifying forest canopy traits: Imaging
864 spectroscopy versus field survey. *Remote Sensing of Environment*, 158, 15-27
- 865 Asner, G.P., Martin, R.E., Knapp, D.E., Tupayachi, R., Anderson, C.B., Sinca, F., Vaughn, N.R., & Llactayo,
866 W. (2017). Airborne laser-guided imaging spectroscopy to map forest trait diversity and guide
867 conservation. *Science*, 355, 385
- 868 Bae, S., Levick, S.R., Heidrich, L., Magdon, P., Leutner, B.F., Wöllauer, S., Serebryanyk, A., Nauss, T.,
869 Krzystek, P., Gossner, M.M., Schall, P., Heibl, C., Bäessler, C., Doerfler, I., Schulze, E.-D., Krah, F.-S.,
870 Culmsee, H., Jung, K., Heurich, M., Fischer, M., Seibold, S., Thorn, S., Gerlach, T., Hothorn, T., Weisser,

871 W.W., & Müller, J. (2019). Radar vision in the mapping of forest biodiversity from space. *Nature*
872 *Communications*, 10, 4757

873 Baeten, L., Verheyen, K., Wirth, C., Bruelheide, H., Bussotti, F., Finér, L., Jaroszewicz, B., Selvi, F.,
874 Valladares, F., Allan, E., Ampoorter, E., Auge, H., Avăcăriei, D., Barbaro, L., Bărnoaiea, I., Bastias, C.C.,
875 Bauhus, J., Beinhoff, C., Benavides, R., Benneter, A., Berger, S., Berthold, F., Boberg, J., Bonal, D.,
876 Brüggemann, W., Carnol, M., Castagneyrol, B., Charbonnier, Y., Čečko, E., Coomes, D., Coppi, A.,
877 Dalmaris, E., Dănilă, G., Dawud, S.M., de Vries, W., De Wandeler, H., Deconchat, M., Domisch, T.,
878 Duduman, G., Fischer, M., Fotelli, M., Gessler, A., Gimeno, T.E., Granier, A., Grossiord, C., Guyot, V.,
879 Hantsch, L., Hättenschwiler, S., Hector, A., Hermy, M., Holland, V., Jactel, H., Joly, F.-X., Jucker, T.,
880 Kolb, S., Koricheva, J., Lexer, M.J., Liebergesell, M., Milligan, H., Müller, S., Muys, B., Nguyen, D.,
881 Nichiforel, L., Pollastrini, M., Proulx, R., Rabasa, S., Radoglou, K., Ratcliffe, S., Raulund-Rasmussen,
882 K., Seiferling, I., Stenlid, J., Vesterdal, L., von Wilpert, K., Zavala, M.A., Zielinski, D., & Scherer-
883 Lorenzen, M. (2013). A novel comparative research platform designed to determine the functional
884 significance of tree species diversity in European forests. *Perspectives in Plant Ecology, Evolution and*
885 *Systematics*, 15, 281-291

886 Barnosky, A.D., Matzke, N., Tomiya, S., Wogan, G.O.U., Swartz, B., Quental, T.B., Marshall, C., McGuire,
887 J.L., Lindsey, E.L., Maguire, K.C., Mersey, B., & Ferrer, E.A. (2011). Has the Earth's sixth mass
888 extinction already arrived? *Nature*, 471, 51-57

889 Bayat, B., van der Tol, C., & Verhoef, W. (2018). Integrating satellite optical and thermal infrared
890 observations for improving daily ecosystem functioning estimations during a drought episode. *Remote*
891 *Sensing of Environment*, 209, 375-394

892 Benavides, R., Scherer-Lorenzen, M., & Valladares, F. (2019a). The functional trait space of tree species is
893 influenced by the species richness of the canopy and the type of forest. *Oikos*, 128, 1435-1445

894 Benavides, R., Valladares, F., Wirth, C., Müller, S., & Scherer-Lorenzen, M. (2019b). Intraspecific trait
895 variability of trees is related to canopy species richness in European forests. *Perspectives in Plant Ecology,*
896 *Evolution and Systematics*, 36, 24-32

897 Botta-Dukát, Z. (2005). Rao's quadratic entropy as a measure of functional diversity based on multiple
898 traits. *Journal of Vegetation Science*, 16, 533-540

899 Brodu, N. (2017). Super-Resolving Multiresolution Images With Band-Independent Geometry of
900 Multispectral Pixels. *IEEE Transactions on Geoscience and Remote Sensing*, 55, 4610-4617

901 Cavender-Bares, J., Gamon, J.A., & Townsend, P.A. (2020). The Use of Remote Sensing to Enhance
902 Biodiversity Monitoring and Detection: A Critical Challenge for the Twenty-First Century. In J. Cavender-
903 Bares, J.A. Gamon, & P.A. Townsend (Eds.), *Remote Sensing of Plant Biodiversity* (pp. 1-12). Cham:
904 Springer International Publishing

905 Ceballos, G., Ehrlich, P.R., Barnosky, A.D., García, A., Pringle, R.M., & Palmer, T.M. (2015). Accelerated
906 modern human-induced species losses: Entering the sixth mass extinction. *Science Advances*, 1,
907 e1400253

908 Celesti, M., van der Tol, C., Cogliati, S., Panigada, C., Yang, P., Pinto, F., Rascher, U., Miglietta, F.,
909 Colombo, R., & Rossini, M. (2018). Exploring the physiological information of Sun-induced chlorophyll
910 fluorescence through radiative transfer model inversion. *Remote Sensing of Environment*, 215, 97-108

911 Coyle, D., Stysley, P., Poullos, D., Clarke, G., & Kay, R. (2015). Laser transmitter development for NASA's
912 Global Ecosystem Dynamics Investigation (GEDI) lidar. *SPIE*

913 Dalponte, M., Bruzzone, L., Vescovo, L., & Gianelle, D. (2009). The role of spectral resolution and
914 classifier complexity in the analysis of hyperspectral images of forest areas. *Remote Sensing of*
915 *Environment*, 113, 2345-2355

916 Darvishzadeh, R., Skidmore, A., Schlerf, M., & Atzberger, C. (2008). Inversion of a radiative transfer model
917 for estimating vegetation LAI and chlorophyll in a heterogeneous grassland. *Remote Sensing of*
918 *Environment*, 112, 2592-2604

919 Dempster, A.P., Laird, N.M., & Rubin, D.B. (1977). Maximum Likelihood from Incomplete Data via the
920 EM Algorithm. *Journal of the Royal Statistical Society. Series B (Methodological)*, 39, 1-38

921 Díaz, S., & Cabido, M. (2001). Vive la différence: plant functional diversity matters to ecosystem processes.
922 *Trends in Ecology & Evolution*, 16, 646-655

923 Drusch, M., Del Bello, U., Carlier, S., Colin, O., Fernandez, V., Gascon, F., Hoersch, B., Isola, C., Laberinti,
924 P., Martimort, P., Meygret, A., Spoto, F., Sy, O., Marchese, F., & Bargellini, P. (2012). Sentinel-2: ESA's
925 Optical High-Resolution Mission for GMES Operational Services. *Remote Sensing of Environment*, 120,
926 25-36

927 ESA, 2017. Sentinel-2 Spectral Response Functions (S2-SRF).
928 [https://sentinels.copernicus.eu/web/sentinel/user-guides/sentinel-2-msi/document-library/-](https://sentinels.copernicus.eu/web/sentinel/user-guides/sentinel-2-msi/document-library/-/asset_publisher/Wk0TKajiISaR/content/sentinel-2a-spectral-responses)
929 [/asset_publisher/Wk0TKajiISaR/content/sentinel-2a-spectral-responses](https://sentinels.copernicus.eu/web/sentinel/user-guides/sentinel-2-msi/document-library/-/asset_publisher/Wk0TKajiISaR/content/sentinel-2a-spectral-responses) (accessed 7 December 2021)

930 Evans, J.R., & Clarke, V.C. (2019). The nitrogen cost of photosynthesis. *Journal of Experimental Botany*,
931 70, 7-15

932 Fassnacht, F.E., Müllerová, J., Conti, L., Malavasi, M., & Schmidlein, S. (2022). About the link between
933 biodiversity and spectral variation. *Applied Vegetation Science*, 25, e12643

934 Fauvel, M., Lopes, M., Dubo, T., Rivers-Moore, J., Frison, P.-L., Gross, N., & Ouin, A. (2020). Prediction
935 of plant diversity in grasslands using Sentinel-1 and -2 satellite image time series. *Remote Sensing of*
936 *Environment*, 237, 111536

937 Feilhauer, H., Zlinszky, A., Kania, A., Foody, G.M., Doktor, D., Lausch, A., & Schmidlein, S. (2021). Let
938 your maps be fuzzy!—Class probabilities and floristic gradients as alternatives to crisp mapping for
939 remote sensing of vegetation. *Remote Sensing in Ecology and Conservation*, 7, 292-305

940 Féret, J.-B., & Asner, G.P. (2014). Mapping tropical forest canopy diversity using high-fidelity imaging
941 spectroscopy. *Ecological Applications*, 24, 1289-1296

942 Feret, J.-B., François, C., Asner, G.P., Gitelson, A.A., Martin, R.E., Bidet, L.P.R., Ustin, S.L., le Maire, G.,
943 & Jacquemoud, S. (2008). PROSPECT-4 and 5: Advances in the leaf optical properties model separating
944 photosynthetic pigments. *Remote Sensing of Environment*, 112, 3030-3043

945 Féret, J.B., Gitelson, A.A., Noble, S.D., & Jacquemoud, S. (2017). PROSPECT-D: Towards modeling leaf
946 optical properties through a complete lifecycle. *Remote Sensing of Environment*, 193, 204-215

947 Fischer, F.J., Maréchaux, I., & Chave, J. (2019). Improving plant allometry by fusing forest models and
948 remote sensing. *New Phytologist*, 223, 1159-1165

949 Gamon, J.A., Wang, R., Gholizadeh, H., Zutta, B., Townsend, P.A., & Cavender-Bares, J. (2020).
950 Consideration of Scale in Remote Sensing of Biodiversity. In J. Cavender-Bares, J.A. Gamon, & P.A.
951 Townsend (Eds.), *Remote Sensing of Plant Biodiversity* (pp. 425-447). Cham: Springer International
952 Publishing

953 GCOS (2003). The second report on the adequacy of the global observing systems for climate in support of
954 the UNFCCC. In, *GCOS Report* (p. 73). Geneva, Switzerland: World Meteorological Organization

955 Gholizadeh, H., Gamon, J.A., Townsend, P.A., Zygielbaum, A.I., Helzer, C.J., Hmimina, G.Y., Yu, R.,
956 Moore, R.M., Schweiger, A.K., & Cavender-Bares, J. (2019). Detecting prairie biodiversity with airborne
957 remote sensing. *Remote Sensing of Environment*, 221, 38-49

958 Gholizadeh, H., Gamon, J.A., Zygielbaum, A.I., Wang, R., Schweiger, A.K., & Cavender-Bares, J. (2018).
959 Remote sensing of biodiversity: Soil correction and data dimension reduction methods improve
960 assessment of α -diversity (species richness) in prairie ecosystems. *Remote Sensing of Environment*, 206,
961 240-253

962 Goetz, A.F.H. (2009). Three decades of hyperspectral remote sensing of the Earth: A personal view. *Remote*
963 *Sensing of Environment*, 113, S5-S16

964 Gómez-Dans, J.L., Lewis, P.E., & Disney, M. (2016). Efficient Emulation of Radiative Transfer Codes
965 Using Gaussian Processes and Application to Land Surface Parameter Inferences. *Remote Sensing*, 8, 119

966 Gould, K.S. (2004). Nature's Swiss Army Knife: The Diverse Protective Roles of Anthocyanins in Leaves.
967 *Journal of biomedicine & biotechnology*, 2004, 314-320

968 Grossiord, C., Granier, A., Ratcliffe, S., Bouriaud, O., Bruelheide, H., Chećko, E., Forrester, D.I., Dawud,
969 S.M., Finér, L., Pollastrini, M., Scherer-Lorenzen, M., Valladares, F., Bonal, D., & Gessler, A. (2014).
970 Tree diversity does not always improve resistance of forest ecosystems to drought. *Proceedings of the*
971 *National Academy of Sciences*, 111, 14812

972 Hardisty, A.R., Michener, W.K., Agosti, D., Alonso García, E., Bastin, L., Belbin, L., Bowser, A., Buttigieg,
973 P.L., Canhos, D.A.L., Egloff, W., De Giovanni, R., Figueira, R., Groom, Q., Guralnick, R.P., Hobern, D.,
974 Hugo, W., Koureas, D., Ji, L., Los, W., Manuel, J., Manset, D., Poelen, J., Saarenmaa, H., Schigel, D.,
975 Uhlir, P.F., & Kissling, W.D. (2019). The Bari Manifesto: An interoperability framework for essential
976 biodiversity variables. *Ecological Informatics*, 49, 22-31

977 Hauser, L.T., Féret, J.-B., An Binh, N., van der Windt, N., Sil, Â.F., Timmermans, J., Soudzilovskaia, N.A.,
978 & van Bodegom, P.M. (2021a). Towards scalable estimation of plant functional diversity from Sentinel-
979 2: In-situ validation in a heterogeneous (semi-)natural landscape. *Remote Sensing of Environment*, 262,
980 112505

981 Hauser, L.T., Timmermans, J., van der Windt, N., Sil, Â.F., César de Sá, N., Soudzilovskaia, N.A., & van
982 Bodegom, P.M. (2021b). Explaining discrepancies between spectral and in-situ plant diversity in
983 multispectral satellite earth observation. *Remote Sensing of Environment*, 265, 112684

984 Heumann, B.W., Hackett, R.A., & Monfils, A.K. (2015). Testing the spectral diversity hypothesis using
985 spectroscopy data in a simulated wetland community. *Ecological Informatics*, 25, 29-34

986 Hosgood, B., Jacquemoud, S., Andreoli, G., Verdebout, J., Pedrini, G., & Schmuck, G. (1994). Leaf Optical
987 Properties Experiment 93 (LOPEX93). In E.C.J.R. Centre (Ed.). Ispra (Italy). Available online:
988 [http://opticleaf.ipgp.fr/databases/LDB_lopex1993.xls], last accessed 11-Nov-2020

989 Houborg, R., & Anderson, M. (2009). Utility of an image-based canopy reflectance modeling tool for
990 remote estimation of LAI and leaf chlorophyll content at regional scales. In (p. 29): SPIE

991 Hughes, N.M., Morley, C.B., & Smith, W.K. (2007). Coordination of anthocyanin decline and
992 photosynthetic maturation in juvenile leaves of three deciduous tree species. *New Phytologist*, 175, 675-
993 685

994 Ibarrola-Ulzurrun, E., Drumetz, L., Marcello, J., Gonzalo-Martín, C., & Chanussot, J. (2019). Hyperspectral
995 Classification Through Unmixing Abundance Maps Addressing Spectral Variability. *IEEE Transactions*
996 *on Geoscience and Remote Sensing*, 57, 4775-4788

997 Jacquemoud, S., & Baret, F. (1990). PROSPECT: A model of leaf optical properties spectra. *Remote*
998 *Sensing of Environment*, 34, 75-91

999 Jacquemoud, S., Verhoef, W., Baret, F., Bacour, C., Zarco-Tejada, P.J., Asner, G.P., François, C., & Ustin,
1000 S.L. (2009). PROSPECT+SAIL models: A review of use for vegetation characterization. *Remote Sensing*
1001 *of Environment*, 113, S56-S66

1002 Jetz, W., Cavender-Bares, J., Pavlick, R., Schimel, D., Davis, F.W., Asner, G.P., Guralnick, R., Kattge, J.,
1003 Latimer, A.M., Moorcroft, P., Schaepman, M.E., Schildhauer, M.P., Schneider, F.D., Schrodtt, F., Stahl,
1004 U., & Ustin, S.L. (2016). Monitoring plant functional diversity from space. *Nature Plants*, 2, 16024

1005 Jetz, W., McGeoch, M.A., Guralnick, R., Ferrier, S., Beck, J., Costello, M.J., Fernandez, M., Geller, G.N.,
1006 Keil, P., Merow, C., Meyer, C., Muller-Karger, F.E., Pereira, H.M., Regan, E.C., Schmeller, D.S., & Turak,
1007 E. (2019). Essential biodiversity variables for mapping and monitoring species populations. *Nature*
1008 *Ecology & Evolution*, 3, 539-551

1009 Jucker, T., Bongalov, B., Burslem, D.F.R.P., Nilus, R., Dalponte, M., Lewis, S.L., Phillips, O.L., Qie, L., &
1010 Coomes, D.A. (2018). Topography shapes the structure, composition and function of tropical forest
1011 landscapes. *Ecology Letters*, 21, 989-1000

1012 Kattenborn, T., & Schmidlein, S. (2019). Radiative transfer modelling reveals why canopy reflectance
1013 follows function. *Scientific Reports*, 9, 6541

1014 Kerr, G., Avbelj, J., Carmona, E., Eckardt, A., Gerasch, B., Graham, L., Günther, B., Heiden, U., Krutz, D.,
1015 Krawczyk, H., Makarau, A., Miller, R., Müller, R., Perkins, R., & Walter, I. (2016). The hyperspectral
1016 sensor DESIS on MUSES: Processing and applications. In, 2016 IEEE International Geoscience and
1017 Remote Sensing Symposium (IGARSS) (pp. 268-271)

1018 Kerr, J.T., & Ostrovsky, M. (2003). From space to species: ecological applications for remote sensing.
1019 *Trends in Ecology & Evolution*, 18, 299-305

1020 Laliberté, E., & Legendre, P. (2010). A distance-based framework for measuring functional diversity from
1021 multiple traits. *Ecology*, 91, 299-305

1022 Laliberté, E., Schweiger, A.K., & Legendre, P. (2020). Partitioning plant spectral diversity into alpha and
1023 beta components. *Ecology Letters*, 23, 370-380

1024 Lee, K.-S., Cohen, W.B., Kennedy, R.E., Maier-sperger, T.K., & Gower, S.T. (2004). Hyperspectral versus
1025 multispectral data for estimating leaf area index in four different biomes. *Remote Sensing of Environment*,
1026 91, 508-520

1027 Lu, B., He, Y., & Dao, P.D. (2019). Comparing the Performance of Multispectral and Hyperspectral Images
1028 for Estimating Vegetation Properties. *IEEE Journal of Selected Topics in Applied Earth Observations and*
1029 *Remote Sensing*, 12, 1784-1797

1030 Ma, X., Mahecha, M.D., Migliavacca, M., van der Plas, F., Benavides, R., Ratcliffe, S., Kattge, J., Richter,
1031 R., Musavi, T., Baeten, L., Barnoiaica, I., Bohn, F.J., Bouriaud, O., Bussotti, F., Coppi, A., Domisch, T.,
1032 Huth, A., Jaroszewicz, B., Joswig, J., Pabon-Moreno, D.E., Papale, D., Selvi, F., Laurin, G.V., Valladares,

1033 F., Reichstein, M., & Wirth, C. (2019). Inferring plant functional diversity from space: the potential of
1034 Sentinel-2. *Remote Sensing of Environment*, 233, 111368

1035 Ma, X., Migliavacca, M., Wirth, C., Bohn, J.F., Huth, A., Richter, R., & Mahecha, D.M. (2020). Monitoring
1036 Plant Functional Diversity Using the Reflectance and Echo from Space. *Remote Sensing*, 12

1037 Manetas, Y. (2006). Why some leaves are anthocyanic and why most anthocyanic leaves are red? *Flora -*
1038 *Morphology, Distribution, Functional Ecology of Plants*, 201, 163-177

1039 Mason, N.W.H., Mouillot, D., Lee, W.G., & Wilson, J.B. (2005). Functional richness, functional evenness
1040 and functional divergence: the primary components of functional diversity. *Oikos*, 111, 112-118

1041 Mattila, H., Valev, D., Havurinne, V., Khorobrykh, S., Virtanen, O., Antinluoma, M., Mishra, K.B., &
1042 Tyystjärvi, E. (2018). Degradation of chlorophyll and synthesis of flavonols during autumn senescence—
1043 the story told by individual leaves. *AoB PLANTS*, 10

1044 Melville, B., Lucieer, A., & Aryal, J. (2019). Classification of Lowland Native Grassland Communities
1045 Using Hyperspectral Unmanned Aircraft System (UAS) Imagery in the Tasmanian Midlands. *Drones*, 3

1046 Mouchet, M.A., Villéger, S., Mason, N.W.H., & Mouillot, D. (2010). Functional diversity measures: an
1047 overview of their redundancy and their ability to discriminate community assembly rules. *Functional*
1048 *Ecology*, 24, 867-876

1049 Nagendra, H. (2001). Using remote sensing to assess biodiversity. *International Journal of Remote Sensing*,
1050 22, 2377-2400

1051 Nagendra, H., & Rocchini, D. (2008). High resolution satellite imagery for tropical biodiversity studies: the
1052 devil is in the detail. *Biodiversity and Conservation*, 17, 3431

1053 North, P.R.J. (1996). Three-dimensional forest light interaction model using a Monte Carlo method. *IEEE*
1054 *Transactions on Geoscience and Remote Sensing*, 34, 946-956

1055 Pacheco-Labrador, J., El-Madany, T.S., van der Tol, C., Martin, M.P., Gonzalez-Cascon, R., Perez-Priego,
1056 O., Guan, J., Moreno, G., Carrara, A., Reichstein, M., & Migliavacca, M. (2021). senSCOPE: Modeling

1057 mixed canopies combining green and brown senesced leaves. Evaluation in a Mediterranean Grassland.
1058 Remote Sensing of Environment, 257, 112352

1059 Palmer, M.W., Earls, P.G., Hoagland, B.W., White, P.S., & Wohlgenuth, T. (2002). Quantitative tools for
1060 perfecting species lists. Environmetrics, 13, 121-137

1061 Pearson, K. (1901). LIII. On lines and planes of closest fit to systems of points in space. The London,
1062 Edinburgh, and Dublin Philosophical Magazine and Journal of Science, 2, 559-572

1063 Pedregosa, F., Varoquaux, G., Gramfort, A., Michel, V., Thirion, B., Grisel, O., Blondel, M., Prettenhofer,
1064 P., Weiss, R., Dubourg, V., Vanderplas, J., Passos, A., Cournapeau, D., Brucher, M., Perrot, M., &
1065 Duchesnay, É. (2011). Scikit-learn: Machine Learning in Python. Journal of Machine Learning Research,
1066 12, 2825-2830

1067 Pereira, H.M., Ferrier, S., Walters, M., Geller, G.N., Jongman, R.H.G., Scholes, R.J., Bruford, M.W.,
1068 Brummitt, N., Butchart, S.H.M., Cardoso, A.C., Coops, N.C., Dulloo, E., Faith, D.P., Freyhof, J., Gregory,
1069 R.D., Heip, C., Höft, R., Hurtt, G., Jetz, W., Karp, D.S., McGeoch, M.A., Obura, D., Onoda, Y., Pettorelli,
1070 N., Reyers, B., Sayre, R., Scharlemann, J.P.W., Stuart, S.N., Turak, E., Walpole, M., & Wegmann, M.
1071 (2013). Essential Biodiversity Variables. Science, 339, 277

1072 Pereira, H.M., Navarro, L.M., & Martins, I.S. (2012). Global Biodiversity Change: The Bad, the Good, and
1073 the Unknown. Annual Review of Environment and Resources, 37, 25-50

1074 Peters, R.D., & Noble, S.D. (2020). Sensitivity and Correlation Analysis of PROSPECT-D and ABM-B
1075 Leaf Models. IEEE Transactions on Geoscience and Remote Sensing, 1-10

1076 Pourcel, L., Routaboul, J.-M., Cheynier, V., Lepiniec, L., & Debeaujon, I. (2007). Flavonoid oxidation in
1077 plants: from biochemical properties to physiological functions. Trends in Plant Science, 12, 29-36

1078 Reich, P.B. (2014). The world-wide ‘fast–slow’ plant economics spectrum: a traits manifesto. Journal of
1079 Ecology, 102, 275-301

1080 Rocchini, D., Balkenhol, N., Carter, G.A., Foody, G.M., Gillespie, T.W., He, K.S., Kark, S., Levin, N.,
1081 Lucas, K., Luoto, M., Nagendra, H., Oldeland, J., Ricotta, C., Southworth, J., & Neteler, M. (2010).
1082 Remotely sensed spectral heterogeneity as a proxy of species diversity: Recent advances and open
1083 challenges. *Ecological Informatics*, 5, 318-329

1084 Rocchini, D., Marcantonio, M., Da Re, D., Bacaro, G., Feoli, E., Foody, G.M., Furrer, R., Harrigan, R.J.,
1085 Kleijn, D., Iannacito, M., Lenoir, J., Lin, M., Malavasi, M., Marchetto, E., Meyer, R.S., Moudry, V.,
1086 Schneider, F.D., Šimová, P., Thornhill, A.H., Thouverai, E., Vicario, S., Wayne, R.K., & Ricotta, C.
1087 (2021). From zero to infinity: Minimum to maximum diversity of the planet by spatio-parametric Rao's
1088 quadratic entropy. *Global Ecology and Biogeography*, 30, 1153-1162

1089 Rossi, C., Kneubühler, M., Schütz, M., Schaepman, M.E., Haller, R.M., & Risch, A.C. (2020). From local
1090 to regional: Functional diversity in differently managed alpine grasslands. *Remote Sensing of*
1091 *Environment*, 236, 111415

1092 Schneider, F.D., Morsdorf, F., Schmid, B., Petchey, O.L., Hueni, A., Schimel, D.S., & Schaepman, M.E.
1093 (2017). Mapping functional diversity from remotely sensed morphological and physiological forest traits.
1094 *Nature Communications*, 8, 1441

1095 Scholes, R.J., Walters, M., Turak, E., Saarenmaa, H., Heip, C.H.R., Tuama, É.Ó., Faith, D.P., Mooney, H.A.,
1096 Ferrier, S., Jongman, R.H.G., Harrison, I.J., Yahara, T., Pereira, H.M., Larigauderie, A., & Geller, G.
1097 (2012). Building a global observing system for biodiversity. *Current Opinion in Environmental*
1098 *Sustainability*, 4, 139-146

1099 Schweiger, A.K., Cavender-Bares, J., Townsend, P.A., Hobbie, S.E., Madritch, M.D., Wang, R., Tilman, D.,
1100 & Gamon, J.A. (2018). Plant spectral diversity integrates functional and phylogenetic components of
1101 biodiversity and predicts ecosystem function. *Nature Ecology & Evolution*, 2, 976-982

1102 Shannon, C.E. (1948). A Mathematical Theory of Communication. *Bell System Technical Journal*, 27, 379-
1103 423

1104 Simonson, W.D., Allen, H.D., & Coomes, D.A. (2014). Applications of airborne lidar for the assessment of
1105 animal species diversity. *Methods in Ecology and Evolution*, 5, 719-729

1106 Skidmore, A.K., Coops, N.C., Neinavaz, E., Ali, A., Schaepman, M.E., Paganini, M., Kissling, W.D.,
1107 Vihervaara, P., Darvishzadeh, R., Feilhauer, H., Fernandez, M., Fernández, N., Gorelick, N.,
1108 Geijzendorffer, I., Heiden, U., Heurich, M., Hobern, D., Holzwarth, S., Muller-Karger, F.E., Van De
1109 Kerchove, R., Lausch, A., Leitão, P.J., Lock, M.C., Múcher, C.A., O'Connor, B., Rocchini, D., Roeoesli,
1110 C., Turner, W., Vis, J.K., Wang, T., Wegmann, M., & Wingate, V. (2021). Priority list of biodiversity
1111 metrics to observe from space. *Nature Ecology & Evolution*, 5, 896-906

1112 Sluiter, R., & Pebesma, E.J. (2010). Comparing techniques for vegetation classification using multi- and
1113 hyperspectral images and ancillary environmental data. *International Journal of Remote Sensing*, 31,
1114 6143-6161

1115 Small, C., & Sousa, D. (2016). Humans on Earth: Global extents of anthropogenic land cover from remote
1116 sensing. *Anthropocene*, 14, 1-33

1117 Sohl, T., & Sleeter, B. (2012). Role of Remote Sensing for Land-Use and Land-Cover Change Modeling.
1118 In C.P. Giri (Ed.), *Remote sensing of land use and land cover: principles and applications* (pp. 225-239).
1119 Boca Raton, FL: CRC Press

1120 Stagakis, S., Vanikiotis, T., & Sykioti, O. (2016). Estimating forest species abundance through linear
1121 unmixing of CHRIS/PROBA imagery. *ISPRS Journal of Photogrammetry and Remote Sensing*, 119, 79-
1122 89

1123 Stein, A., Gerstner, K., & Kreft, H. (2014). Environmental heterogeneity as a universal driver of species
1124 richness across taxa, biomes and spatial scales. *Ecology Letters*, 17, 866-880

1125 Sun, Y., Huang, J., Ao, Z., Lao, D., & Xin, Q. (2019). Deep Learning Approaches for the Mapping of Tree
1126 Species Diversity in a Tropical Wetland Using Airborne LiDAR and High-Spatial-Resolution Remote
1127 Sensing Images. *Forests*, 10, 1047

1128 Tagliabue, G., Panigada, C., Celesti, M., Cogliati, S., Colombo, R., Migliavacca, M., Rascher, U., Rocchini,
1129 D., Schüttemeyer, D., & Rossini, M. (2020). Sun-induced fluorescence heterogeneity as a measure of
1130 functional diversity. *Remote Sensing of Environment*, 247, 111934

1131 Torres, R., Snoeij, P., Geudtner, D., Bibby, D., Davidson, M., Attema, E., Potin, P., Rommen, B., Floury,
1132 N., Brown, M., Traver, I.N., Deghaye, P., Duesmann, B., Rosich, B., Miranda, N., Bruno, C., L'Abbate,
1133 M., Croci, R., Pietropaolo, A., Huchler, M., & Rostan, F. (2012). GMES Sentinel-1 mission. *Remote
1134 Sensing of Environment*, 120, 9-24

1135 Torresani, M., Feilhauer, H., Rocchini, D., Féret, J.-B., Zebisch, M., & Tonon, G. (2021). Which optical
1136 traits enable an estimation of tree species diversity based on the Spectral Variation Hypothesis? *Applied
1137 Vegetation Science*, 24, e12586

1138 Torresani, M., Rocchini, D., Sonnenschein, R., Zebisch, M., Marcantonio, M., Ricotta, C., & Tonon, G.
1139 (2019). Estimating tree species diversity from space in an alpine conifer forest: The Rao's Q diversity
1140 index meets the spectral variation hypothesis. *Ecological Informatics*, 52, 26-34

1141 Turner, D.P., Acker, S.A., Means, J.E., & Garman, S.L. (2000). Assessing alternative allometric algorithms
1142 for estimating leaf area of Douglas-fir trees and stands. *Forest Ecology and Management*, 126, 61-76

1143 Turner, W., Spector, S., Gardiner, N., Fladeland, M., Sterling, E., & Steininger, M. (2003). Remote sensing
1144 for biodiversity science and conservation. *Trends in Ecology & Evolution*, 18, 306-314

1145 Ustin, S.L., & Gamon, J.A. (2010). Remote sensing of plant functional types. *New Phytologist*, 186, 795-
1146 816

1147 Valbuena, R., O'Connor, B., Zellweger, F., Simonson, W., Vihervaara, P., Maltamo, M., Silva, C.A.,
1148 Almeida, D.R.A., Danks, F., Morsdorf, F., Chirici, G., Lucas, R., Coomes, D.A., & Coops, N.C. (2020).
1149 Standardizing Ecosystem Morphological Traits from 3D Information Sources. *Trends in Ecology &
1150 Evolution*, 35, 656-667

1151 Van Cleemput, E., Helsen, K., Feilhauer, H., Honnay, O., & Somers, B. (2021). Spectrally defined plant
1152 functional types adequately capture multidimensional trait variation in herbaceous communities.
1153 *Ecological Indicators*, 120, 106970

1154 van den Berg, R.A., Hoefsloot, H.C.J., Westerhuis, J.A., Smilde, A.K., & van der Werf, M.J. (2006).
1155 Centering, scaling, and transformations: improving the biological information content of metabolomics
1156 data. In, *BMC genomics* (p. 142)

1157 van der Tol, C., Verhoef, W., Timmermans, J., Verhoef, A., & Su, Z. (2009). An integrated model of soil-
1158 canopy spectral radiances, photosynthesis, fluorescence, temperature and energy balance.
1159 *Biogeosciences*, 6, 3109-3129

1160 Verhoef, W. (1985). Earth observation modeling based on layer scattering matrices. *Remote Sensing of*
1161 *Environment*, 17, 165-178

1162 Vilfan, N., Van der Tol, C., Yang, P., Wyber, R., Malenovský, Z., Robinson, S.A., & Verhoef, W. (2018).
1163 Extending Fluspect to simulate xanthophyll driven leaf reflectance dynamics. *Remote Sensing of*
1164 *Environment*, 211, 345-356

1165 Villéger, S., Mason, N.W.H., & Mouillot, D. (2008). New multidimensional functional diversity indices for
1166 a multifaceted framework in functional ecology. *Ecology*, 89, 2290-2301

1167 Wang, R., & Gamon, J.A. (2019). Remote sensing of terrestrial plant biodiversity. *Remote Sensing of*
1168 *Environment*, 231, 111218

1169 Wang, R., Gamon, J.A., Cavender-Bares, J., Townsend, P.A., & Zygielbaum, A.I. (2018a). The spatial
1170 sensitivity of the spectral diversity–biodiversity relationship: an experimental test in a prairie grassland.
1171 *Ecological Applications*, 28, 541-556

1172 Wang, R., Gamon, J.A., Schweiger, A.K., Cavender-Bares, J., Townsend, P.A., Zygielbaum, A.I., & Kothari,
1173 S. (2018b). Influence of species richness, evenness, and composition on optical diversity: A simulation
1174 study. *Remote Sensing of Environment*, 211, 218-228

1175 Warren, S.D., Alt, M., Olson, K.D., Irl, S.D.H., Steinbauer, M.J., & Jentsch, A. (2014). The relationship
1176 between the spectral diversity of satellite imagery, habitat heterogeneity, and plant species richness.
1177 *Ecological Informatics*, 24, 160-168

1178 Wright, I.J., Reich, P.B., Westoby, M., Ackerly, D.D., Baruch, Z., Bongers, F., Cavender-Bares, J., Chapin,
1179 T., Cornelissen, J.H.C., Diemer, M., Flexas, J., Garnier, E., Groom, P.K., Gulias, J., Hikosaka, K., Lamont,
1180 B.B., Lee, T., Lee, W., Lusk, C., Midgley, J.J., Navas, M.-L., Niinemets, Ü., Oleksyn, J., Osada, N.,
1181 Poorter, H., Poot, P., Prior, L., Pyankov, V.I., Roumet, C., Thomas, S.C., Tjoelker, M.G., Veneklaas, E.J.,
1182 & Villar, R. (2004). The worldwide leaf economics spectrum. *Nature*, 428, 821

1183 Yang, J., Gong, P., Fu, R., Zhang, M., Chen, J., Liang, S., Xu, B., Shi, J., & Dickinson, R. (2013). The role
1184 of satellite remote sensing in climate change studies. *Nature Climate Change*, 3, 875-883

1185 Zhao, M., Tian, S., Zhu, Y., Li, Z., Zeng, S., & Liu, S. (2021). Allometric relationships, functional
1186 differentiations, and scaling of growth rates across 151 tree species in China. *Ecosphere*, 12, e03522

1187 Zhao, Y., Zeng, Y., Zheng, Z., Dong, W., Zhao, D., Wu, B., & Zhao, Q. (2018). Forest species diversity
1188 mapping using airborne LiDAR and hyperspectral data in a subtropical forest in China. *Remote Sensing*
1189 *of Environment*, 213, 104-114

1190 Zhu, C., Byrd, R.H., Lu, P., & Nocedal, J. (1997). Algorithm 778: L-BFGS-B: Fortran subroutines for large-
1191 scale bound-constrained optimization. *ACM Trans. Math. Softw.*, 23, 550–560

1192